

# Full-Duplex MIMO Relaying: Achievable Rates under Limited Dynamic Range

Brian P. Day,\* Adam R. Margetts,† Daniel W. Bliss,† and Philip Schniter\*‡

## Abstract

In this paper we consider the problem of full-duplex multiple-input multiple-output (MIMO) relaying between a source and destination who do not share a direct link. The principal difficulty in implementing such a system is that, due to the limited attenuation between the relay's transmit and receive antenna arrays, the relay's outgoing signal may overwhelm its limited-dynamic-range input circuitry, making it difficult—if not impossible—to recover the desired incoming signal. While explicitly modeling transmitter/receiver dynamic-range limitations and channel estimation error, we derive tight upper and lower bounds on the end-to-end achievable rate of decode-and-forward-based full-duplex MIMO relay systems, and propose a transmission scheme based on maximization of the lower bound. The maximization requires us to (numerically) solve a nonconvex optimization problem, for which we detail a novel approach based on bisection search and gradient projection. To gain insights into system design tradeoffs, we also derive an analytic approximation to the achievable rate and numerically demonstrate its accuracy. We then study the behavior of the achievable rate as a function of signal-to-noise ratio, interference-to-noise ratio, transmitter/receiver dynamic range, number of antennas, and training length, using optimized half-duplex signaling as a baseline.

*Keywords:* MIMO relays, full-duplex relays, limited dynamic range, channel estimation.

\*Brian Day and Philip Schniter are with the Department of Electrical and Computer Engineering, The Ohio State University, Columbus, OH.

†Daniel Bliss and Adam Margetts are with the Advanced Sensor Techniques Group, MIT Lincoln Laboratory, Lexington, MA.

‡Please direct all correspondence to Prof. Philip Schniter, Dept. ECE, The Ohio State University, 2015 Neil Ave., Columbus OH 43210, e-mail: schniter@ece.osu.edu, phone 614.247.6488, fax 614.292.7596.

This work was sponsored by the United States Air Force under Air Force contract FA8721-05-C-0002. Opinions, interpretations, conclusions, and recommendations are those of the authors and are not necessarily endorsed by the United States Government.

## I. INTRODUCTION

We consider the problem of communicating from a source node to a destination node, who do not share a direct link, through a relay node. Traditional relay systems operate in a *half-duplex* mode, whereby the time-frequency signal-space used for the source-to-relay link is kept orthogonal to that used for the relay-to-destination link, such as with non-overlapping time periods or frequency bands. Half-duplex operation is used to avoid the high levels of relay self-interference that are faced with *full-duplex* operation (see Fig. 1), where the source and relay share a common time-frequency signal-space. For example, it is not unusual for the ratio between the relay’s self-interference power and desired incoming signal power to exceed 100 dB [1], or—in general—some value larger than the dynamic range of the relay’s front-end hardware, making it impossible to recover the desired signal. The importance of *limited dynamic-range* (DR) cannot be overstressed; notice that, even if the self-interference signal was perfectly known, limited-DR renders perfect cancellation impossible.

Recently, *multiple-input multiple-output* (MIMO) relaying has been proposed as a means of increasing spectral efficiency (e.g., [2], [3]). By MIMO relaying, we mean that the source, relay, and destination each use multiple antennas for both reception and transmission. MIMO relaying brings the possibility of full-duplex operation through *spatial* self-interference suppression (e.g., [1], [4]–[13]). As a simple example, one can imagine using the relay’s transmit array to form spatial nulls at a subset of the relay’s receive antennas, which are then free of self-interference and able to recover the desired signal. In forming these nulls, however, it can be seen that the relay consumes spatial degrees-of-freedom that could have been used in communicating data to the destination. Thus, maximizing the end-to-end throughput involves navigating a tradeoff between the source-to-relay link and relay-to-destination link. Of course, maximizing end-to-end throughput is more involved than simply protecting an arbitrary subset of the relay’s receive antennas; one also needs to consider which subset to protect, and the degree to which each of those antennas are protected, given the source-to-relay and relay-to-destination MIMO channel coefficients, the estimation errors on those coefficients, and the DR limitations of the various nodes. These considerations motivate the following fundamental questions about full-duplex MIMO relaying in the presence of self-interference: 1) *What is the maximum achievable end-to-end throughput under a transmit power constraint?* 2) *How can the system be designed to achieve this throughput?*

In this paper, we aim to answer these two fundamental questions while paying special attention to the effects of both limited-DR and channel estimation error.

- 1) Limited-DR is a natural consequence of non-ideal amplifiers, oscillators, analog-to-digital converters

(ADCs), and digital-to-analog converters (DACs). To model the effects of limited receiver-DR, we inject, at each receive antenna, an additive white Gaussian ‘‘receiver distortion’’ with variance  $\beta$  times the energy impinging on that receive antenna (where  $\beta \ll 1$ ). Similarly, to model the effects of limited transmitter-DR, we inject, at each transmit antenna, an additive white Gaussian ‘‘transmitter noise’’ with variance  $\kappa$  times the energy of the intended transmit signal (where  $\kappa \ll 1$ ). Thus,  $\kappa^{-1}$  and  $\beta^{-1}$  characterize the transmitter and receiver dynamic ranges, respectively.

- 2) Imperfect CSI can result for several reasons, including channel time-variation, additive noise, and DR limitations. We focus on CSI imperfections that result from the use of pilot-aided least-squares (LS) channel estimation performed in the presence of limited-DR.

For simplicity, we focus on relay systems without<sup>1</sup> a direct link between the source and destination, which is a reasonable model when those nodes are very far apart. Moreover, we consider regenerative relays that decode-and-forward (as in [1], [4]–[8]), as opposed to simpler non-regenerative relays that only amplify-and-forward (as in [9]–[13]).

The contributions of this paper are as follows. For the full-duplex MIMO relaying problem:

- 1) an explicit model for transmitter/receiver-DR limitations is proposed;
- 2) pilot-aided least-squares MIMO-channel estimation, under DR limitations, is analyzed;
- 3) the residual self-interference, from DR limitations and channel-estimation error, is analyzed;
- 4) lower and upper bounds on the achievable rate are derived;
- 5) a transmission scheme is proposed based on maximizing the achievable-rate lower bound subject to a power constraint, requiring the solution of a nonconvex optimization problem, to which we apply bisection search and Gradient Projection;
- 6) an analytic approximation of the maximum achievable rate is proposed; and,
- 7) the achievable rate is numerically investigated as a function of signal-to-noise ratio, interference-to-noise ratio, transmitter/receiver dynamic range, number of antennas, and number of pilots.

*Notation:* We use  $(\cdot)^\top$  to denote transpose,  $(\cdot)^*$  conjugate, and  $(\cdot)^\text{H}$  conjugate transpose. For matrices  $\mathbf{A}, \mathbf{B} \in \mathbb{C}^{M \times N}$ , we use  $\text{tr}(\mathbf{A})$  to denote trace,  $\det(\mathbf{A})$  to denote determinant,  $\mathbf{A} \odot \mathbf{B}$  to denote elementwise (i.e., Hadamard) product,  $\text{sum}[\mathbf{A}] \in \mathbb{C}$  to denote the sum over all elements,  $\text{vec}(\mathbf{A}) \in \mathbb{C}^{MN}$  to denote vectorization,  $\text{diag}(\mathbf{A})$  to denote the diagonal matrix with the same diagonal elements as  $\mathbf{A}$ ,  $\text{Diag}(\mathbf{a})$  to denote the diagonal matrix whose diagonal is constructed from the vector  $\mathbf{a}$ , and  $[\mathbf{A}]_{m,n}$  to

<sup>1</sup> The papers [2], [3] study achievable rate in the case that a source-to-destination link exists. However, they ignore relay self-interference, which is the main focus of our paper.

denote the element in the  $m^{th}$  row and  $n^{th}$  column of  $\mathbf{A}$ . We denote expectation by  $\text{E}\{\cdot\}$ , covariance by  $\text{Cov}\{\cdot\}$ , statistical independence by  $\perp\!\!\!\perp$ , the circular complex Gaussian pdf with mean vector  $\mathbf{m}$  and covariance matrix  $\mathbf{Q}$  by  $\mathcal{CN}(\mathbf{m}, \mathbf{Q})$ , and the Kronecker delta by  $\delta_k$ . Finally,  $\mathbf{I}$  denotes the identity matrix,  $\mathbb{C}$  the complex field, and  $\mathbb{Z}$  the integers.

## II. SYSTEM MODEL

We will use  $N_s$  and  $N_r$  to denote the number of transmit antennas at the source and relay, respectively, and  $M_r$  and  $M_d$  to denote the number of receive antennas at the relay and destination, respectively. Here and in the sequel, we use subscript- $s$  for source, subscript- $r$  for relay, and subscript- $d$  for destination. Similarly, we will use subscript- $sr$  for source-to-relay, subscript- $rd$  for relay-to-destination, and subscript- $rr$  for relay-to-relay. At times, we will omit the subscripts when referring to common quantities. For example, we will use  $\mathbf{s}(t) \in \mathbb{C}^N$  to denote the time- $t$  noisy signals radiated by the transmit antenna arrays, and  $\mathbf{u}(t) \in \mathbb{C}^M$  to denote the time- $t$  undistorted signals collected by the receive antenna arrays. More specifically, the source's and relay's radiated signals are  $\mathbf{s}_s(t) \in \mathbb{C}^{N_s}$  and  $\mathbf{s}_r(t) \in \mathbb{C}^{N_r}$ , respectively, while the relay's and destination's collected signals are  $\mathbf{u}_r(t) \in \mathbb{C}^{M_r}$  and  $\mathbf{u}_d(t) \in \mathbb{C}^{M_d}$ , respectively.

### A. Propagation Channels

We assume that propagation between each transmitter-receiver pair can be characterized by a Raleigh-fading MIMO channel  $\mathbf{H} \in \mathbb{C}^{M \times N}$  corrupted by additive white Gaussian noise (AWGN)  $\mathbf{n}(t)$ . By “Rayleigh fading,” we mean that  $\text{vec}(\mathbf{H}) \sim \mathcal{CN}(\mathbf{0}, \mathbf{I}_{MN})$ , and by “AWGN,” we mean that  $\mathbf{n}(t) \sim \mathcal{CN}(\mathbf{0}, \mathbf{I}_M)$ . The time- $t$  radiated signals  $\mathbf{s}(t)$  are then related to the received signals  $\mathbf{u}(t)$  via

$$\mathbf{u}_r(t) = \sqrt{\rho_r} \mathbf{H}_{sr} \mathbf{s}_s(t) + \sqrt{\eta_r} \mathbf{H}_{rr} \mathbf{s}_r(t) + \mathbf{n}_r(t) \quad (1)$$

$$\mathbf{u}_d(t) = \sqrt{\rho_d} \mathbf{H}_{rd} \mathbf{s}_r(t) + \mathbf{n}_d(t). \quad (2)$$

In (1)-(2),  $\rho > 0$  denotes signal-to-noise ratio (SNR), and  $\eta_r > 0$  denotes the relay's interference-to-noise ratio (INR). The INR  $\eta_r$  will depend on the separation between, and orientation of, the relay's transmit and receive antenna arrays [8].

### B. Transmission Protocol

We assume that the signaling epoch  $\mathcal{T}$  is partitioned into a training period  $\mathcal{T}_{\text{train}}$  and a subsequent data communication period  $\mathcal{T}_{\text{data}}$ . For reasons that will become clear in the sequel, the training period is itself partitioned into two equal-length portions (i.e.,  $\mathcal{T}_{\text{train}}[1]$  and  $\mathcal{T}_{\text{train}}[2]$ ), as is the data period (i.e.,

$\mathcal{T}_{\text{data}}[1]$  and  $\mathcal{T}_{\text{data}}[2]$ ). Within each of these four sub-periods, we assume that the transmitted signals are zero-mean and wide-sense stationary.

### C. Limited Transmitter Dynamic Range

We model the effect of limited transmitter dynamic range (DR) by injecting, per transmit antenna, an independent zero-mean Gaussian ‘‘transmitter noise’’ whose variance is  $\kappa$  times the energy of the *intended* transmit signal at that antenna. In particular, say that  $\mathbf{x}(t) \in \mathbb{C}^N$  denotes the transmitter’s intended time- $t$  transmit signal, and say  $\mathbf{Q} \triangleq \text{Cov}\{\mathbf{x}(t)\}$  over the relevant time period (e.g.,  $t \in \mathcal{T}_{\text{data}}[1]$ ). We then write the time- $t$  noisy radiated signal as

$$\mathbf{s}(t) = \mathbf{x}(t) + \mathbf{c}(t) \text{ s.t. } \begin{cases} \mathbf{c}(t) \sim \mathcal{CN}(\mathbf{0}, \kappa \text{diag}(\mathbf{Q})) \\ \mathbf{c}(t) \perp\!\!\!\perp \mathbf{x}(t) \\ \mathbf{c}(t) \perp\!\!\!\perp \mathbf{c}(t') \big|_{t' \neq t} \end{cases}, \quad (3)$$

where  $\mathbf{c}(t) \in \mathbb{C}^N$  denotes the transmitter noise. Typically,  $\kappa \ll 1$ . The model (3) closely approximates the combined effects of additive power-amp noise, non-linearities in the DAC and power-amp, and oscillator phase noise (e.g., [14]).

### D. Limited Receiver Dynamic Range

We model the effect of limited receiver-DR by injecting, per receive antenna, an independent zero-mean Gaussian ‘‘receiver distortion’’ whose variance is  $\beta$  times the energy collected by that antenna. In particular, say that  $\mathbf{u}(t) \in \mathbb{C}^M$  denotes the receiver’s undistorted time- $t$  received vector, and say  $\Phi_i \triangleq \text{Cov}\{\mathbf{u}(t)\}$  over the relevant time period (e.g.,  $t \in \mathcal{T}_{\text{data}}[1]$ ). We then write the distorted post-ADC received signal as

$$\mathbf{y}(t) = \mathbf{u}(t) + \mathbf{e}(t) \text{ s.t. } \begin{cases} \mathbf{e}(t) \sim \mathcal{CN}(\mathbf{0}, \beta \text{diag}(\Phi)) \\ \mathbf{e}(t) \perp\!\!\!\perp \mathbf{u}(t) \\ \mathbf{e}(t) \perp\!\!\!\perp \mathbf{e}(t') \big|_{t' \neq t} \end{cases}, \quad (4)$$

where  $\mathbf{e}(t) \in \mathbb{C}^M$  is additive distortion. Typically,  $\beta \ll 1$ . The model (4) closely approximates the combined effects of additive gain-control noise, non-linearities in the ADC and gain-control, and oscillator phase noise (e.g., [15]).

Figure 2 summarizes our model. The dashed lines indicate that the distortion levels are proportional to mean energy levels and not to the instantaneous value.

### III. ANALYSIS OF ACHIEVABLE RATE

In this work, we consider systems that use the transmission protocol from Section II-B, pilot-aided channel estimation (as described in Section III-A), and partial self-interference cancellation at the relay (as described in Section III-B). For such systems, we derive upper and lower bounds on achievable rate (in Section III-C), and we propose a novel signal design based on optimization of the achievable-rate lower-bound subject to a power constraint (in Section IV). To better understand the behavior of the optimized achievable rate, we derive a simple approximation (in Section V) that is shown (in Section VI) to be reasonably accurate, on average.

#### A. Pilot-Aided Channel Estimation

In this section, we describe the pilot-aided channel estimation procedure that is used to learn the channel matrices  $\mathbf{H}$ . In our protocol, the training interval consists of two sub-periods,  $\mathcal{T}_{\text{train}}[1]$  and  $\mathcal{T}_{\text{train}}[2]$ , each of duration  $TN$  channel uses (for some  $T \in \mathbb{Z}^+$ ). For all times  $t \in \mathcal{T}_{\text{train}}[1]$ , we assume that the source transmits a known pilot signal and the relay remains silent, while, for all  $t \in \mathcal{T}_{\text{train}}[2]$ , the relay transmits and the source remains silent. As we shall see, it suffices to choose the pilot sequences  $\mathbf{X} = [\mathbf{x}(1), \dots, \mathbf{x}(TN)] \in \mathbb{C}^{N \times TN}$  arbitrarily so long as they satisfy  $\frac{1}{2T} \mathbf{X} \mathbf{X}^H = \mathbf{I}_N$ , where the scaling is chosen to satisfy a per-period power constraint of the form  $\text{tr}(\mathbf{Q}) = 2$ , consistent with the data power constraints that will be described in the sequel.

Our limited transmitter/receiver-DR model implies that the (distorted) space-time pilot signal observed by a given receiver takes the form

$$\mathbf{Y} = \sqrt{\alpha} \mathbf{H}(\mathbf{X} + \mathbf{C}) + \mathbf{N} + \mathbf{E}, \quad (5)$$

where  $\alpha \in \{\rho_r, \eta_r, \rho_d\}$  for  $\mathbf{H} \in \{\mathbf{H}_{\text{sr}}, \mathbf{H}_{\text{rr}}, \mathbf{H}_{\text{rd}}\}$ , respectively. In (5),  $\mathbf{C}, \mathbf{E}$  and  $\mathbf{N}$  are  $N \times TN$  matrices of transmitter noise, receiver distortion, and AWGN, respectively. At the conclusion of training, we assume that each receiver uses least-squares (LS) to estimate the corresponding channel  $\mathbf{H}$  as

$$\sqrt{\alpha} \hat{\mathbf{H}} \triangleq \frac{1}{2T} \mathbf{Y} \mathbf{X}^H, \quad (6)$$

and communicates this estimate to the transmitter through a side channel.<sup>2</sup> In the sequel, it will be useful to decompose the channel estimate into the true channel plus an estimation error. In Appendix A, it is

<sup>2</sup> For our achievable-rate analysis, we assume the channel is fixed for a long time, making negligible the relative overhead required for CSI exchange.

shown that such a decomposition takes the form

$$\sqrt{\alpha} \hat{\mathbf{H}} = \sqrt{\alpha} \mathbf{H} + \mathbf{D}^{\frac{1}{2}} \tilde{\mathbf{H}}, \quad (7)$$

where the entries of  $\tilde{\mathbf{H}}$  are i.i.d  $\mathcal{CN}(0, 1)$ , and where

$$\mathbf{D} = \frac{1}{2T} [(1 + \beta) \mathbf{I} + \alpha \frac{2\kappa}{N} \mathbf{H} \mathbf{H}^H + \alpha \frac{2\beta}{N} (1 + \kappa) \text{diag}(\mathbf{H} \mathbf{H}^H)] \quad (8)$$

characterizes the spatial covariance of the estimation error. Using  $\beta \ll 1$  and  $\kappa \ll 1$ , this covariance reduces to

$$\mathbf{D} \approx \frac{1}{2T} [\mathbf{I} + \alpha \frac{2\kappa}{N} \mathbf{H} \mathbf{H}^H + \alpha \frac{2\beta}{N} \text{diag}(\mathbf{H} \mathbf{H}^H)]. \quad (9)$$

### B. Interference Cancellation and Equivalent Channel

We now describe how the relay partially cancels its self-interference, and construct a simplified model for the result.

Recall that the data communication period is partitioned into two sub-periods,  $\mathcal{T}_{\text{data}}[1]$  and  $\mathcal{T}_{\text{data}}[2]$ , and that—within each—the transmitted signals are wide-sense stationary. Thus, at any time  $t \in \mathcal{T}_{\text{data}}[l]$ , the relay's (instantaneous, distorted) signal takes the form

$$\mathbf{y}_r[l] = (\sqrt{\rho_r} \hat{\mathbf{H}}_{sr} - \mathbf{D}_{sr}^{\frac{1}{2}} \tilde{\mathbf{H}}_{sr})(\mathbf{x}_s[l] + \mathbf{c}_s[l]) + \mathbf{n}_r[l] + \mathbf{e}_r[l] + (\sqrt{\eta_r} \hat{\mathbf{H}}_{rr} - \mathbf{D}_{rr}^{\frac{1}{2}} \tilde{\mathbf{H}}_{rr})(\mathbf{x}_r[l] + \mathbf{c}_r[l]), \quad (10)$$

as implied by Fig. 2 and (7). Collecting the unknown interference components of (10) into

$$\mathbf{v}_r[l] \triangleq \sqrt{\rho_r} \hat{\mathbf{H}}_{sr} \mathbf{c}_s[l] - \mathbf{D}_{sr}^{\frac{1}{2}} \tilde{\mathbf{H}}_{sr} (\mathbf{x}_s[l] + \mathbf{c}_s[l]) + \mathbf{n}_r[l] + \mathbf{e}_r[l], + \sqrt{\eta_r} \hat{\mathbf{H}}_{rr} \mathbf{c}_r[l] - \mathbf{D}_{rr}^{\frac{1}{2}} \tilde{\mathbf{H}}_{rr} (\mathbf{x}_r[l] + \mathbf{c}_r[l]) \quad (11)$$

we can write  $\mathbf{y}_r[l] = \sqrt{\rho_r} \hat{\mathbf{H}}_{sr} \mathbf{x}_s[l] + \sqrt{\eta_r} \hat{\mathbf{H}}_{rr} \mathbf{x}_r[l] + \mathbf{v}_r[l]$ , where the self-interference term  $\sqrt{\eta_r} \hat{\mathbf{H}}_{rr} \mathbf{x}_r[l]$  is known and thus can be canceled. The interference-canceled signal  $\mathbf{z}_r[l] \triangleq \mathbf{y}_r[l] - \sqrt{\eta_r} \hat{\mathbf{H}}_{rr} \mathbf{x}_r[l]$  can then be written as

$$\mathbf{z}_r[l] = \sqrt{\rho_r} \hat{\mathbf{H}}_{sr} \mathbf{x}_s[l] + \mathbf{v}_r[l]. \quad (12)$$

Equation (12) shows that, in effect, the information signal  $\mathbf{x}_s[l]$  propagates through a known channel  $\sqrt{\rho_r} \hat{\mathbf{H}}_{sr}$  corrupted by an aggregate (possibly non-Gaussian) noise  $\mathbf{v}_r[l]$ , whose  $(\hat{\mathbf{H}}_{sr}, \hat{\mathbf{H}}_{rr})$ -conditional covariance we denote as  $\hat{\Sigma}_r[l] \triangleq \text{Cov}\{\mathbf{v}_r[l] | \hat{\mathbf{H}}_{sr}, \hat{\mathbf{H}}_{rr}\}$ . In Appendix B, we show that

$$\begin{aligned} \hat{\Sigma}_r[l] \approx \mathbf{I} + \kappa \rho_r \hat{\mathbf{H}}_{sr} \text{diag}(\mathbf{Q}_s[l]) \hat{\mathbf{H}}_{sr}^H + \hat{\mathbf{D}}_{sr} \text{tr}(\mathbf{Q}_s[l]) + \kappa \eta_r \hat{\mathbf{H}}_{rr} \text{diag}(\mathbf{Q}_r[l]) \hat{\mathbf{H}}_{rr}^H + \hat{\mathbf{D}}_{rr} \text{tr}(\mathbf{Q}_r[l]) \\ + \beta \rho_r \text{diag}(\hat{\mathbf{H}}_{sr} \mathbf{Q}_s[l] \hat{\mathbf{H}}_{sr}^H) + \beta \eta_r \text{diag}(\hat{\mathbf{H}}_{rr} \mathbf{Q}_r[l] \hat{\mathbf{H}}_{rr}^H), \end{aligned} \quad (13)$$

where  $\hat{\mathbf{D}}_{\text{sr}} \triangleq \text{E}\{\mathbf{D}_{\text{sr}} | \hat{\mathbf{H}}_{\text{sr}}\}$  and  $\hat{\mathbf{D}}_{\text{rr}} \triangleq \text{E}\{\mathbf{D}_{\text{rr}} | \hat{\mathbf{H}}_{\text{rr}}\}$  obey

$$\hat{\mathbf{D}} \approx \frac{1}{2T} [\mathbf{I} + \alpha \frac{2\kappa}{N} \hat{\mathbf{H}} \hat{\mathbf{H}}^H + \alpha \frac{2\beta}{N} \text{diag}(\hat{\mathbf{H}} \hat{\mathbf{H}}^H)] \quad (14)$$

and where the approximations in (13)-(14) follow from  $\kappa \ll 1$  and  $\beta \ll 1$ . We note, for later, that the channel estimation error terms  $\hat{\mathbf{D}}$  can be made arbitrarily small through appropriate choice of  $T$ .

The effective channel from the relay to the destination can be similarly stated as

$$\mathbf{v}_{\text{d}}[l] \triangleq \sqrt{\rho_{\text{d}}} \mathbf{H}_{\text{rd}} \mathbf{c}_{\text{r}}[l] - \mathbf{D}_{\text{rd}}^{\frac{1}{2}} \hat{\mathbf{H}}_{\text{rd}} \mathbf{x}_{\text{r}}[l] + \mathbf{n}_{\text{d}}[l] + \mathbf{e}_{\text{d}}[l] \quad (15)$$

$$\mathbf{y}_{\text{d}}[l] = \sqrt{\rho_{\text{d}}} \hat{\mathbf{H}}_{\text{rd}} \mathbf{x}_{\text{r}}[l] + \mathbf{v}_{\text{d}}[l], \quad (16)$$

where (15) lacks the self-interference component present in (11), and an expression similar to (13) can be derived for  $\hat{\Sigma}_{\text{d}}[l]$ . Figure 3 summarizes the equivalent system model.

### C. Bounds on Achievable Rate

The end-to-end mutual information can be written as [2]

$$I(\mathbf{Q}) = \min \left\{ \frac{1}{2} \sum_{l=1}^2 I_{\text{sr}}(\mathbf{Q}[l]), \frac{1}{2} \sum_{l=1}^2 I_{\text{rd}}(\mathbf{Q}[l]) \right\}, \quad (17)$$

where  $I_{\text{sr}}(\mathbf{Q}[l])$  and  $I_{\text{rd}}(\mathbf{Q}[l])$  are the subperiod- $l$  mutual informations of the source-to-relay channel and relay-to-destination channel, respectively, and where  $\mathbf{Q}[l] \triangleq (\mathbf{Q}_{\text{s}}[l], \mathbf{Q}_{\text{r}}[l])$  and  $\mathbf{Q} \triangleq (\mathbf{Q}[1], \mathbf{Q}[2])$ .

To analyze  $I_{\text{sr}}(\mathbf{Q}[l])$  and  $I_{\text{rd}}(\mathbf{Q}[l])$ , we leverage the equivalent system model shown in Fig. 3. Still, the mutual-information analysis is complicated by the fact that the aggregate noises  $\mathbf{v}_{\text{r}}[l]$  and  $\mathbf{v}_{\text{d}}[l]$  are generally non-Gaussian, as a result of the channel-estimation-error components in (11) and (15). However, it is known that, among all noise distributions of a given covariance, the Gaussian one is worst from a mutual-information perspective [16]. In particular, treating the noise as Gaussian yields the lower bounds  $I_{\text{sr}}(\mathbf{Q}[l]) \geq \underline{I}_{\text{sr}}(\mathbf{Q}[l])$  and  $I_{\text{rd}}(\mathbf{Q}[l]) \geq \underline{I}_{\text{rd}}(\mathbf{Q}[l])$ , where [17]

$$\begin{aligned} \underline{I}_{\text{sr}}(\mathbf{Q}[l]) &= \log \det (\mathbf{I} + \rho_{\text{r}} \hat{\mathbf{H}}_{\text{sr}} \mathbf{Q}_{\text{s}}[l] \hat{\mathbf{H}}_{\text{sr}}^H \hat{\Sigma}_{\text{r}}^{-1}[l]) \\ &= \log \det (\rho_{\text{r}} \hat{\mathbf{H}}_{\text{sr}} \mathbf{Q}_{\text{s}}[l] \hat{\mathbf{H}}_{\text{sr}}^H + \hat{\Sigma}_{\text{r}}[l]) - \log \det (\hat{\Sigma}_{\text{r}}[l]) \end{aligned} \quad (18)$$

$$\begin{aligned} \underline{I}_{\text{rd}}(\mathbf{Q}[l]) &= \log \det (\mathbf{I} + \rho_{\text{d}} \hat{\mathbf{H}}_{\text{rd}} \mathbf{Q}_{\text{r}}[l] \hat{\mathbf{H}}_{\text{rd}}^H \hat{\Sigma}_{\text{r}}^{-1}[l]) \\ &= \log \det (\rho_{\text{d}} \hat{\mathbf{H}}_{\text{rd}} \mathbf{Q}_{\text{r}}[l] \hat{\mathbf{H}}_{\text{rd}}^H + \hat{\Sigma}_{\text{d}}[l]) - \log \det (\hat{\Sigma}_{\text{d}}[l]), \end{aligned} \quad (19)$$

and thus a lower bound on the end-to-end achievable-rate

$$\underline{I}(\mathbf{Q}) = \min \left\{ \underbrace{\frac{1}{2} \sum_{l=1}^2 \underline{I}_{\text{sr}}(\mathbf{Q}[l])}_{\triangleq \underline{I}_{\text{sr}}(\mathbf{Q})}, \underbrace{\frac{1}{2} \sum_{l=1}^2 \underline{I}_{\text{rd}}(\mathbf{Q}[l])}_{\triangleq \underline{I}_{\text{rd}}(\mathbf{Q})} \right\}. \quad (20)$$

Moreover, the rate  $\underline{I}(\mathcal{Q})$  bits<sup>3</sup>-per-channel-use (bpcu) can be achieved via independent Gaussian codebooks at the transmitters and maximum-likelihood detection at the receivers [17].

A straightforward achievable-rate upper bound  $\overline{I}(\mathcal{Q})$  results from the case of perfect CSI (i.e.,  $\hat{\mathbf{D}} = \mathbf{0}$ ), where  $\mathbf{v}_r[l]$  and  $\mathbf{v}_d[l]$  are Gaussian. Moreover, the lower bound  $\underline{I}(\mathcal{Q})$  converges to the upper bound  $\overline{I}(\mathcal{Q})$  as the training  $T \rightarrow \infty$ .

#### IV. TRANSMIT COVARIANCE OPTIMIZATION

We would now like to find the transmit covariance matrices  $\mathcal{Q}$  that maximize the achievable-rate lower bound  $\underline{I}(\mathcal{Q})$  in (20) subject to the per-link power constraint  $\mathcal{Q} \in \mathbb{Q}$ , where

$$\mathbb{Q} \triangleq \left\{ \mathcal{Q} \text{ s.t. } \frac{1}{2} \sum_{l=1}^2 \text{tr}(\mathbf{Q}_s[l]) \leq 1, \frac{1}{2} \sum_{l=1}^2 \text{tr}(\mathbf{Q}_r[l]) \leq 1, \right. \\ \left. \mathbf{Q}_s[l] \geq 0, \mathbf{Q}_r[l] \geq 0, \mathbf{Q}_s[l] = \mathbf{Q}_s^H[l], \mathbf{Q}_r[l] = \mathbf{Q}_r^H[l] \right\}. \quad (21)$$

We note that optimizing the transmit covariance matrices is equivalent to jointly optimizing the transmission beam-patterns and power levels. In the sequel, we denote the optimal (i.e., maximin) rate by

$$\underline{I}_* \triangleq \max_{\mathcal{Q} \in \mathbb{Q}} \min \{ \underline{I}_{sr}(\mathcal{Q}), \underline{I}_{rd}(\mathcal{Q}) \}, \quad (22)$$

and we use  $\mathbb{Q}_*$  to denote the corresponding set of maximin designs  $\mathcal{Q}$  (which are, in general, not unique).

##### A. Weighted-Sum-Rate Optimization

It is important to realize that, among the maximin designs  $\mathbb{Q}_*$ , there exists at least one “link-equalizing” design, i.e.,  $\exists \mathcal{Q} \in \mathbb{Q}_* \text{ s.t. } \underline{I}_{sr}(\mathcal{Q}) = \underline{I}_{rd}(\mathcal{Q})$ . To see why this is the case, notice that, given any maximin design  $\mathcal{Q}$  such that  $\underline{I}_{sr}(\mathcal{Q}) > \underline{I}_{rd}(\mathcal{Q})$ , a simple scaling of  $\mathbf{Q}_s[l]$  can yield  $\underline{I}_{sr}(\mathcal{Q}) = \underline{I}_{rd}(\mathcal{Q})$ , and thus an equalizing design. A similar argument can be made when  $\underline{I}_{rd}(\mathcal{Q}) > \underline{I}_{sr}(\mathcal{Q})$ .

Referring to the set of *all* link-equalizing designs (maximin or otherwise) as

$$\mathbb{Q}_- \triangleq \{ \mathcal{Q} \in \mathbb{Q} \text{ s.t. } \underline{I}_{sr}(\mathcal{Q}) = \underline{I}_{rd}(\mathcal{Q}) \}, \quad (23)$$

the maximin equalizing design can be found by solving  $\arg \max_{\mathcal{Q} \in \mathbb{Q}_-} \underline{I}_{sr}(\mathcal{Q})$  or  $\arg \max_{\mathcal{Q} \in \mathbb{Q}_-} \underline{I}_{rd}(\mathcal{Q})$ , where the equivalence is due to the equalizing property. More generally, the maximin equalizing design can be found by solving

$$\arg \max_{\mathcal{Q} \in \mathbb{Q}_-} \underline{I}(\mathcal{Q}, \zeta) \quad (24)$$

<sup>3</sup> Throughout the paper, we take “log” to be base-2.

with any fixed  $\zeta \in (0, 1)$  and the  $\zeta$ -weighted sum-rate

$$\underline{I}(\mathcal{Q}, \zeta) \triangleq \frac{\zeta}{2} \underline{I}_{\text{sr}}(\mathcal{Q}) + \frac{1-\zeta}{2} \underline{I}_{\text{rd}}(\mathcal{Q}). \quad (25)$$

To find the maximin equalizing design, we propose relaxing the constraint on  $\mathcal{Q}$  from  $\mathbb{Q}_-$  to  $\mathbb{Q}$ , yielding the  $\zeta$ -weighted-sum-rate optimization problem

$$\mathcal{Q}_*(\zeta) = \arg \max_{\mathcal{Q} \in \mathbb{Q}} \underline{I}(\mathcal{Q}, \zeta). \quad (26)$$

Now, if there exists  $\zeta_- \in (0, 1)$  such that the solution  $\mathcal{Q}_*(\zeta_-)$  to (26) is link-equalizing, then, because  $\mathbb{Q}_- \subset \mathbb{Q}$ , we know that  $\mathcal{Q}_*(\zeta_-)$  must also solve the problem (24), implying that  $\mathcal{Q}_*(\zeta_-)$  is maximin. Figure 4(a) illustrates the case where such a  $\zeta_-$  exists. It may be, however, that no  $\zeta \in (0, 1)$  yields a link-equalizing solution  $\mathcal{Q}_*(\zeta)$ , as illustrated in Fig. 4(b). This case occurs when  $\underline{I}_{\text{sr}}(\mathcal{Q}_*(\zeta)) > \underline{I}_{\text{rd}}(\mathcal{Q}_*(\zeta))$  for all  $\zeta \in (0, 1)$ , such as when  $\rho_r \gg \rho_d$ . In this latter case, the maximin rate reduces to  $\underline{I}_* = \lim_{\zeta \rightarrow 0} \underline{I}_{\text{rd}}(\mathcal{Q}_*(\zeta))$ .

Whether or not  $\zeta_- \in (0, 1)$  actually exists, we propose to search for  $\zeta_-$  using bisection, leveraging the fact that  $\underline{I}_{\text{rd}}(\mathcal{Q}_*(\zeta))$  is non-increasing in  $\zeta$  and  $\underline{I}_{\text{sr}}(\mathcal{Q}_*(\zeta))$  is non-decreasing in  $\zeta$ . To perform the bisection search, we initialize the search interval  $\mathcal{I}$  at  $(0, 1)$ , and bisect it at each step after testing the condition  $\underline{I}_{\text{rd}}(\mathcal{Q}_*(\zeta)) > \underline{I}_{\text{sr}}(\mathcal{Q}_*(\zeta))$  at the midpoint location  $\zeta$  in  $\mathcal{I}$ ; if the condition holds true, we discard the left sub-interval of  $\mathcal{I}$ , else we discard the right sub-interval. We stop bisecting when  $|\underline{I}_{\text{rd}}(\mathcal{Q}_*(\zeta)) - \underline{I}_{\text{sr}}(\mathcal{Q}_*(\zeta))|$  falls below a threshold or a maximum number of iterations has elapsed. Notice that, even when there exists no  $\zeta_- \in (0, 1)$ , bisection converges towards the desired weight  $\zeta = 0$ .

### B. Gradient Projection

At each bisection step, we use Gradient Projection (GP) to solve<sup>4</sup> the  $\zeta$ -weighted-sum-rate optimization problem (26). The GP algorithm [18] is defined as follows. For the generic problem of maximizing a function  $f(\mathbf{x})$  over  $\mathbf{x} \in \mathcal{X}$ , the GP algorithm starts with an initialization  $\mathbf{x}^{(0)}$  and iterates the following steps for  $k = 0, 1, 2, 3, \dots$

$$\tilde{\mathbf{x}}^{(k)} = \mathcal{P}_{\mathcal{X}}(\mathbf{x}^{(k)} + s^{(k)} \nabla f(\mathbf{x}^{(k)})) \quad (27)$$

$$\mathbf{x}^{(k+1)} = \mathbf{x}^{(k)} + \gamma^{(k)} (\tilde{\mathbf{x}}^{(k)} - \mathbf{x}^{(k)}), \quad (28)$$

<sup>4</sup> Because (22) is generally non-convex, finding the global maximum can be difficult. Although GP is guaranteed only to find a local, and not global, maximum, our experience with different initializations suggests that GP is indeed finding the global maximum in our problem.

where  $\mathcal{P}_{\mathcal{X}}(\cdot)$  denotes projection onto the set  $\mathcal{X}$  and  $\nabla f(\cdot)$  denotes the gradient of  $f(\cdot)$ . The parameters  $\gamma^{(k)} \in (0, 1]$  and  $s^{(k)}$  act as stepsizes. In the sequel, we assume  $s^{(k)} = 1 \forall k$ .

In applying GP to the optimization problem (26), we first take gradient steps for  $\mathbf{Q}_r[1]$  and  $\mathbf{Q}_r[2]$ , and then project onto the constraint set (21). Next, we take gradient steps for  $\mathbf{Q}_s[1]$  and  $\mathbf{Q}_s[2]$ , and then project onto the constraint set. In summary, denoting the relay gradient by  $\mathbf{G}_r[l] \triangleq \nabla_{\mathbf{Q}_r[l]} \underline{I}(\mathbf{Q}, \zeta)$  and projection onto (21) by  $\mathcal{P}_{\mathcal{X}}(\cdot)$ , our GP algorithm iterates the following steps to convergence:

$$\mathbf{P}_r^{(k)}[1] = \mathbf{Q}_r^{(k)}[1] + \mathbf{G}_r^{(k)}[1] \quad (29)$$

$$\mathbf{P}_r^{(k)}[2] = \mathbf{Q}_r^{(k)}[2] + \mathbf{G}_r^{(k)}[2] \quad (30)$$

$$(\tilde{\mathbf{Q}}_r^{(k)}[1], \tilde{\mathbf{Q}}_r^{(k)}[2]) = \mathcal{P}_{\mathcal{X}}(\mathbf{P}_r^{(k)}[1], \mathbf{P}_r^{(k)}[2]) \quad (31)$$

$$\mathbf{Q}_r^{(k+1)}[1] = \mathbf{Q}_r^{(k)}[1] + \gamma^{(k)}(\tilde{\mathbf{Q}}_r^{(k)}[1] - \mathbf{Q}_r^{(k)}[1]) \quad (32)$$

$$\mathbf{Q}_r^{(k+1)}[2] = \mathbf{Q}_r^{(k)}[2] + \gamma^{(k)}(\tilde{\mathbf{Q}}_r^{(k)}[2] - \mathbf{Q}_r^{(k)}[2]) \quad (33)$$

and then repeats similar steps for  $\mathbf{Q}_s[1]$  and  $\mathbf{Q}_s[2]$ . An outer loop then repeats this pair of inner loops until the maximum change in  $\mathbf{Q}$  is below a small positive threshold  $\epsilon$ .

We now provide additional details on the GP steps. As for the gradient, Appendix C shows that

$$\begin{aligned} \mathbf{G}_r[l] = & \frac{(1-\zeta)\rho_d}{\ln 2} \left\{ \hat{\mathbf{H}}_{rd}^H (\mathbf{S}_d^{-1}[l] + \beta \text{diag}(\mathbf{S}_d^{-1}[l] - \hat{\Sigma}_d^{-1}[l])) \hat{\mathbf{H}}_{rd} + \text{diag}(\kappa \hat{\mathbf{H}}_{rd}^H (\mathbf{S}_d^{-1}[l] - \hat{\Sigma}_d^{-1}[l]) \hat{\mathbf{H}}_{rd}) \right\} \\ & + \frac{1-\zeta}{\ln 2} \text{sum}(\hat{\mathbf{D}}_{rd}^* \odot (\mathbf{S}_d^{-1}[l] - \hat{\Sigma}_d^{-1}[l])) \mathbf{I} + \frac{\zeta}{\ln 2} \text{sum}(\hat{\mathbf{D}}_{rr}^* \odot (\mathbf{S}_r^{-1}[l] - \hat{\Sigma}_r^{-1}[l])) \mathbf{I} \\ & + \frac{\zeta \eta_r}{\ln 2} \left\{ \text{diag}(\kappa \hat{\mathbf{H}}_{rr}^H (\mathbf{S}_r^{-1}[l] - \hat{\Sigma}_r^{-1}[l]) \hat{\mathbf{H}}_{rr}) + \beta \hat{\mathbf{H}}_{rd}^H \text{diag}(\mathbf{S}_r^{-1}[l] - \hat{\Sigma}_r^{-1}[l]) \hat{\mathbf{H}}_{rd} \right\}, \end{aligned} \quad (34)$$

where

$$\mathbf{S}_d[l] \triangleq \rho_d \hat{\mathbf{H}}_{rd} \mathbf{Q}_r[l] \hat{\mathbf{H}}_{rd}^H + \hat{\Sigma}_d[l] \quad (35)$$

$$\mathbf{S}_r[l] \triangleq \rho_r \hat{\mathbf{H}}_{sr} \mathbf{Q}_s[l] \hat{\mathbf{H}}_{sr}^H + \hat{\Sigma}_r[l]. \quad (36)$$

For  $\mathbf{G}_s[l]$ , a corresponding expression can be derived that is simpler due to lack of self-interference.

To compute the projection  $\mathcal{P}_{\mathcal{X}}(\mathbf{P}_r[1], \mathbf{P}_r[2])$ , we first notice that, due to the Hermitian property of  $\mathbf{P}_r[l]$ , we can construct an eigenvalue decomposition  $\mathbf{P}_r[l] = \mathbf{U}_r[l] \Lambda_r[l] \mathbf{U}_r^H[l]$  with unitary  $\mathbf{U}_r[l]$  and real-valued  $\Lambda_r[l] = \text{Diag}(\lambda_{r,1}[l], \lambda_{r,2}[l], \dots, \lambda_{r,N}[l])$ . The projection of  $(\mathbf{P}_r[1], \mathbf{P}_r[2])$  onto the constraint set (21) then equals  $\tilde{\mathbf{Q}}_r[l] = \mathbf{U}_r[l] (\Lambda_r[l] - \mu \mathbf{I})^+ \mathbf{U}_r^H[l]$ , where  $(\mathbf{B})^+ = \max(\mathbf{B}, \mathbf{0})$  elementwise, and where  $\mu$  is chosen such that  $\frac{1}{2} \sum_{n=1}^N \sum_{l=1}^2 \max(\lambda_{r,n}[l] - \mu, 0) = 1$ . In essence,  $\mathcal{P}_{\mathcal{X}}(\cdot)$  performs water-filling.

To adjust the stepsize  $\gamma^{(k)}$ , we use the Armijo stepsize rule [18], i.e.,  $\gamma^{(k)} = \nu^{m_k}$  where  $m_k$  is the smallest nonnegative integer that satisfies

$$\underline{I}(\mathbf{Q}^{(k+1)}, \zeta) - \underline{I}(\mathbf{Q}^{(k)}, \zeta) \geq \sigma \nu^{m_k} \sum_{l=1}^2 \text{tr} \left( \frac{\zeta}{2} \mathbf{G}_s^{(k)H}[l] (\tilde{\mathbf{Q}}_s^{(k)}[l] - \mathbf{Q}_s^{(k)}[l]) + \frac{1-\zeta}{2} \mathbf{G}_r^{(k)H}[l] (\tilde{\mathbf{Q}}_r^{(k)}[l] - \mathbf{Q}_r^{(k)}[l]) \right)$$

for some constants  $\sigma, \nu$  typically chosen so that  $\sigma \in [10^{-5}, 10^{-1}]$  and  $\nu \in [0.1, 0.5]$ . Above, we used the shorthand  $\mathbf{Q}^{(k)} \triangleq (\mathbf{Q}_s^{(k)}[1], \mathbf{Q}_s^{(k)}[2], \mathbf{Q}_r^{(k)}[1], \mathbf{Q}_r^{(k)}[2])$ .

## V. ACHIEVABLE-RATE APPROXIMATION

The complicated nature of the optimization problem (22) motivates us to approximate its solution, i.e., the covariance-optimized achievable rate  $\underline{I}_* = \max_{\mathbf{Q} \in \mathbb{Q}} \underline{I}(\mathbf{Q})$ . In doing so, we focus on the case of  $T \rightarrow \infty$ , where channel estimation error is driven to zero so that  $\underline{I}(\mathbf{Q}) = I(\mathbf{Q}) = \bar{I}(\mathbf{Q})$ . In addition, for tractability, we restrict ourselves to the case  $N_s = N_r = N$  and  $M_r = M_d = M$ , i.e.,  $N$  transmit antennas at each node, and  $M$  receive antennas at each node.

Our approximation is built around the special case that the channel matrices  $\{\mathbf{H}_{sr}, \mathbf{H}_{rr}, \mathbf{H}_{rd}\}$  are each diagonal, although not necessarily square, and have  $R \triangleq \min\{M, N\}$  identical diagonal entries equal to  $\sqrt{MN/R}$ . (The latter value is chosen so that  $\text{E}\{\text{tr}(\mathbf{H}\mathbf{H}^H)\} = MN$  as assumed in Section II-A.) In this case, the mutual information (20) becomes

$$I(\mathbf{Q}) \approx \min \left\{ \frac{1}{2} \sum_{l=1}^2 \log \det \left( \mathbf{I} + \rho_r \frac{NM}{R} \mathbf{Q}_s[l] (\mathbf{I} + (\kappa + \beta) \frac{NM}{R} [\rho_r \text{diag}(\mathbf{Q}_s[l]) + \eta_r \text{diag}(\mathbf{Q}_r[l])])^{-1} \right), \right. \\ \left. \frac{1}{2} \sum_{l=1}^2 \log \det \left( \mathbf{I} + \rho_d \frac{NM}{R} \mathbf{Q}_r[l] (\mathbf{I} + (\kappa + \beta) \frac{NM}{R} \rho_d \text{diag}(\mathbf{Q}_r[l]))^{-1} \right) \right\}. \quad (37)$$

When  $\eta_r \ll \rho_r$ , the  $\eta_r$ -dependent term in (37) can be ignored, after which it is straightforward to show that, under the constraint (21), the optimal covariances are the ‘‘full duplex’’  $\mathbf{Q}_{FD} \triangleq (\frac{1}{N}\mathbf{I}, \frac{1}{N}\mathbf{I}, \frac{1}{N}\mathbf{I}, \frac{1}{N}\mathbf{I})$ , for which (37) gives

$$I(\mathbf{Q}_{FD}) \approx R \log \left( 1 + \min \left\{ \frac{\rho_r}{\frac{R}{M} + (\kappa + \beta)(\rho_r + \eta_r)}, \frac{\rho_d}{\frac{R}{M} + (\kappa + \beta)\rho_d} \right\} \right) \\ = \begin{cases} R \log \left( 1 + \frac{\rho_d}{\frac{R}{M} + (\kappa + \beta)\rho_d} \right) & \text{if } \frac{\rho_r}{\rho_d} \geq 1 + \frac{(\kappa + \beta)\eta_r M}{R} \\ R \log \left( 1 + \frac{\rho_r}{\frac{R}{M} + (\kappa + \beta)(\rho_r + \eta_r)} \right) & \text{else.} \end{cases} \quad (38)$$

When  $\eta_r \gg \rho_r$ , the  $\eta_r$ -dependent term in (37) dominates unless  $\mathbf{Q}_r[l] = \mathbf{0}$ . In this case, the optimal covariances are the ‘‘half duplex’’ ones  $\mathbf{Q}_{HD} \triangleq (\frac{2}{N}\mathbf{I}, \mathbf{0}, \mathbf{0}, \frac{2}{N}\mathbf{I})$ , for which (37) gives

$$I(\mathbf{Q}_{HD}) \approx \begin{cases} \frac{R}{2} \log \left( 1 + \frac{\rho_d}{\frac{R}{2M} + (\kappa + \beta)\rho_d} \right) & \text{if } \frac{\rho_r}{\rho_d} \geq 1 \\ \frac{R}{2} \log \left( 1 + \frac{\rho_r}{\frac{R}{2M} + (\kappa + \beta)\rho_r} \right) & \text{else.} \end{cases} \quad (39)$$

Finally, given any triple  $(\rho_r, \eta_r, \rho_d)$ , we approximate the achievable rate as follows:  $I_* \approx \max\{I(\mathcal{Q}_{FD}), I(\mathcal{Q}_{HD})\}$ .

From (38)-(39), using  $\theta \triangleq \frac{R}{M(\kappa+\beta)}$ , it is straightforward to show that the approximated system operates as follows.

1) Say  $\frac{\rho_r}{\rho_d} \leq 1$ . Then full-duplex is used iff

$$\eta_r \leq \frac{1}{2} \sqrt{(\theta + 2\rho_r)^2 + \frac{2\rho_r}{\kappa+\beta}(\theta + 2\rho_r)} - \frac{1}{2}\theta. \quad (40)$$

For either half- or full-duplex,  $I_*$  is invariant to  $\rho_d$ , i.e., the source-to-relay link is the limiting one.

2) Say  $1 \leq \frac{\rho_r}{\rho_d} \leq 1 + \frac{(\kappa+\beta)\eta_r M}{R}$ . Full-duplex is used iff

$$\eta_r \leq \frac{\rho_r}{2\rho_d} \sqrt{(\theta + 2\rho_d)^2 + \frac{2\rho_d}{\kappa+\beta}(\theta + 2\rho_d)} - \theta \left(1 - \frac{\rho_r}{2\rho_d}\right). \quad (41)$$

3) Say  $1 + \frac{(\kappa+\beta)\eta_r M}{R} \leq \frac{\rho_r}{\rho_d}$ , or equivalently  $\eta_r \leq \eta_{\text{crit}} \triangleq \left(\frac{\rho_r}{\rho_d} - 1\right) \frac{R}{M(\kappa+\beta)}$ . Then full-duplex is always used, and  $I_*$  is invariant to  $\rho_r$  and  $\eta_r$ , i.e., the rate is limited by the relay-to-destination link.

Figure 5 shows a contour plot of the proposed achievable-rate approximation as a function of INR  $\eta_r$  and SNR  $\rho_r$ , for the case that  $\rho_r/\rho_d = 2$ . We shall see in Section VI that our approximation of the covariance-optimized achievable-rate is reasonably close to that found by solving (22) using bisection/GP.

## VI. NUMERICAL RESULTS

In this section, we numerically investigate the behavior of the end-to-end rates achievable for full-duplex MIMO relaying under the proposed limited transmitter/receiver-DR and channel-estimation-error models. Recall that, in Section III, it was shown that, for a fixed set of transmit covariance matrices  $\mathcal{Q}$ , the achievable rate  $I(\mathcal{Q})$  can be lower-bounded using  $\underline{I}(\mathcal{Q})$  from (20), and upper-bounded using the perfect-CSI  $\bar{I}(\mathcal{Q})$ , where the bounds converge as training  $T \rightarrow \infty$ . Then, in Section IV, a bisection/GP scheme was proposed to maximize  $\underline{I}(\mathcal{Q})$  subject to the power-constraint  $\mathcal{Q} \in \mathbb{Q}$ .

We now study the average behavior of the bisection/GP-optimized rate  $\underline{I}_* = \max_{\mathcal{Q}} \underline{I}(\mathcal{Q})$  as a function of SNRs  $\rho_r$  and  $\rho_d$ ; INR  $\eta_r$ ; dynamic range parameters  $\kappa$  and  $\beta$ ; number of antennas  $N_s, N_r, M_r$ , and  $M_d$ ; and training length  $T$ . We also investigate the role of interference cancellation, the role of two distinct data sub-periods, and the relation to optimized half-duplex (OHD) signaling. In doing so, we find close agreement with the achievable-rate approximation proposed in Section V and illustrated in Fig. 5.

For the numerical results below, the propagation channel model from Section II-A and the limited transmitter/receiver-DR models from Section II-C and Section II-D were employed, pilot-aided channel estimation was implemented as in Section III-A, and the power constraint (21) was applied, implying the channel-estimation-error covariance (8) and the aggregate-noise covariance (13). Throughout, we used

$N \triangleq N_s = N_r$  transmit antennas,  $M \triangleq M_r = M_d$  receive antennas, the SNR ratio  $\rho_r/\rho_d = 2$ , training duration  $T = 50$  (as justified below), Armijo parameters  $\sigma = 0.01$  and  $\nu = 0.2$ , and GP stopping threshold  $\epsilon = 0.01$ . Unless otherwise specified, all results were averaged over 50 realizations.

Below, we denote the full scheme proposed in Section IV by “TCO-2-IC,” which indicates the use of interference cancellation (IC) and transmit covariance optimization (TCO) performed individually over the 2 data sub-periods (i.e.,  $\mathcal{T}_{\text{data}}[1]$  and  $\mathcal{T}_{\text{data}}[2]$ ). To test the impact of IC and of two data sub-periods, we also implemented the proposed scheme but without IC, which we refer to as “TCO-2,” as well as the proposed scheme with only one data sub-period (i.e.,  $\mathbf{Q}_i[1] = \mathbf{Q}_i[2] \forall i$ ), which we refer to as “TCO-1-IC.” To optimize half-duplex, we used GP to maximize the sum-rate  $\underline{I}(\mathbf{Q}, \frac{1}{2})$  under the power constraint (21) and the half-duplex constraint  $\mathbf{Q}_1[2] = \mathbf{0} = \mathbf{Q}_2[1]$ .

To mitigate GP’s sensitivity to initialization, we tried two initializations for each  $\zeta$ -weighted-sum-rate problem, OHD and “naive” full-duplex (NFD), and the one yielding the maximum min-rate was retained. OHD was calculated as explained above, whereas NFD employed non-zero OHD covariance matrices  $\mathbf{Q}_1[1]$  and  $\mathbf{Q}_2[2]$  over both data sub-periods (which would be optimal if  $\eta_r = 0$ ). Note that both OHD and NFD are invariant to both  $\zeta$  and  $\eta_r$ .

In Fig. 6, we investigate the role of channel-estimation training length  $T$  on the achievable-rate lower bound  $\underline{I}(\mathbf{Q})$  of TCO-2-IC. There we see that the rate increases rapidly in  $T$  for small values of  $T$ , but quickly saturates for larger values of  $T$ . This behavior can be understood from (13)-(14), which suggest that channel estimation error will have a negligible effect on the noise covariances  $\hat{\Sigma}_r[l]$  and  $\hat{\Sigma}_d[l]$  when  $TN \gg 1$ . Figure 6 also shows the corresponding achievable-rate upper bounds  $\bar{I}(\mathbf{Q})$ . These traces confirm that the nominal training length  $T = 50$  ensures  $\underline{I}(\mathbf{Q}) \approx \bar{I}(\mathbf{Q}) \approx I(\mathbf{Q})$ .

In Fig. 7, we examine achievable-rate performance versus INR  $\eta_r$  for the TCO-2-IC, TCO-1-IC, TCO-2, and OHD schemes, using different dynamic range parameters  $\beta = \kappa$ . For OHD, we see that rate is invariant to INR  $\eta_r$ , as expected. For the proposed TCO-2-IC, we observe “full duplex” performance for low-to-mid values of  $\eta_r$  and a transition to OHD performance at high values of  $\eta_r$ , just as predicted by the approximation in Section V. In fact, the rates in Fig. 7 are very close to the approximated values in Fig. 5. To see the importance of two distinct data-communication periods, we study the TCO-1-IC trace, where we observe TCO-2-IC-like performance at low-to-mid values of  $\eta_r$ , but performance that drops below OHD at high  $\eta_r$ . Essentially, TCO-1-IC forces full-duplex signaling at high INR  $\eta_r$ , where half-duplex signaling is optimal, while TCO-2-IC facilitates the possibility of half-duplex signaling through the use of two distinct data-communication sub-periods, similar to the MIMO-interference-channel scheme in [19]. Finally, by examining the TCO-2 trace, we conclude that partial interference cancellation is very

important for all but extreme values of INR  $\eta_r$ .

In Fig. 8, we examine the rate of the proposed TCO-IC-2 and OHD versus SNR  $\rho_r$ , using the dynamic range parameters  $\beta = \kappa = -40$ dB and two fixed values of INR  $\eta_r$ . All the behaviors in Fig. 8 are predicted by the rate approximation described in Section V and illustrated in Fig. 5. In particular, at the low INR of  $\eta_r = 20$ dB, TCO-IC-2 operates in the full-duplex regime for all values of SNR  $\rho_r$ . Meanwhile, at the high INR of  $\eta_r = 60$ dB, TCO-IC-2 operates in half-duplex at low values of SNR  $\rho_r$ , but switches to full-duplex after  $\rho_r$  exceeds a threshold.

In Fig. 9, we plot the GP-optimized rate contours of the proposed TCO-IC-2 versus both SNR  $\rho_r$  and INR  $\eta_r$ , for comparison to the approximation in Fig. 5. The two plots show a relatively good match, confirming the accuracy of the approximation. The greatest discrepancy between the plots occurs when  $\eta_r \approx \rho_r$  and both  $\eta_r$  and  $\rho_r$  are large, which makes sense because the approximation was derived using  $\eta_r \ll \rho_r$  and  $\eta_r \gg \rho_r$ .

Finally, in Fig. 10, we explore the achievable rate of TCO-2-IC and OHD versus the number of antennas,  $N$  and  $M$ , for fixed values of SNR  $\rho_r = 15$ dB and  $\rho_r/\rho_d = 2$ , INR  $\eta_r = 40$ dB, and DR parameters  $\beta = \kappa = -40$ dB. We recall, from Fig. 7, that these parameters correspond to the interesting regime where TCO-2-IC performs between half- and full-duplex. In Fig. 10, we see that achievable rate increases with both  $M$  and  $N$  numbers of antennas, as expected. More interesting is the achievable-rate behavior when the total number of antennas per modem is fixed, e.g., at  $N+M = 7$ , as illustrated by the triangles in Fig. 10. The figure indicates that the configurations  $(N, M) = (3, 4)$  and  $(N, M) = (4, 3)$  are best, which (it can be shown) is consistent with approximation from Section V.

## VII. CONCLUSION

We considered the problem of decode-and-forward-based full-duplex MIMO relaying between a source and destination who do not share a direct link. In our analysis, we considered limited transmitter/receiver dynamic range, imperfect CSI, background AWGN, and very high levels of self-interference. Using explicit models for dynamic-range limitation and pilot-aided channel estimation error, we derived upper and lower bounds on the end-to-end achievable rate that tighten as the number of pilots increases. Furthermore, we proposed a transmission scheme based on maximizing the achievable-rate lower-bound. The latter requires the solution to a nonconvex optimization problem, for which we use bisection search and Gradient Projection, the latter of which implicitly performs water-filling. In addition, we derived an analytic approximation to the achievable rate that agrees closely with the results of the numerical optimization. Finally, we studied the achievable-rate numerically, as a function of signal-to-noise ratio,

interference-to-noise ratio, transmitter/receiver dynamic range, number of antennas, and number of pilots. In future work, we plan to investigate the effect of practical coding/decoding schemes, channel time-variation, and bidirectional relaying.

## APPENDIX A CHANNEL ESTIMATION DETAILS

In this appendix, we derive certain details of Section III-A. Under limited transmitter-DR, the undistorted received space-time signal is  $\mathbf{U} = \sqrt{\alpha} \mathbf{H}(\mathbf{X} + \mathbf{C}) + \mathbf{N}$ , where the spatial correlation<sup>5</sup> of the non-distorted pilot signal  $\mathbf{X}$  equals  $\frac{2}{N} \mathbf{I}$  and hence the spatial correlation of the transmitter distortion  $\mathbf{C}$  equals  $\frac{2\kappa}{N} \mathbf{I}$ . Conditioned on  $\mathbf{H}$ , the spatial correlation of  $\mathbf{U}$  is then  $\Phi = \frac{2\alpha(1+\kappa)}{N} \mathbf{H} \mathbf{H}^H + \mathbf{I}$ , and hence the  $\mathbf{H}$ -conditional spatial correlation of the receiver distortion  $\mathbf{E}$  equals  $\beta \text{diag}(\Phi) = \beta \left( \frac{2\alpha(1+\kappa)}{N} \text{diag}(\mathbf{H} \mathbf{H}^H) + \mathbf{I} \right)$ . Given (5), the distorted received signal  $\mathbf{Y}$  can be written as  $\mathbf{Y} = \sqrt{\alpha} \mathbf{H} \mathbf{X} + \mathbf{W}$ , where  $\mathbf{W} \triangleq \sqrt{\alpha} \mathbf{H} \mathbf{C} + \mathbf{N} + \mathbf{E}$  is aggregate complex Gaussian noise that is temporally white with  $\mathbf{H}$ -conditional spatial correlation  $\frac{2\alpha\kappa}{N} \mathbf{H} \mathbf{H}^H + \mathbf{I} + \beta \left( \frac{2\alpha(1+\kappa)}{N} \text{diag}(\mathbf{H} \mathbf{H}^H) + \mathbf{I} \right)$ .

Due to the fact that  $\frac{1}{2T} \mathbf{X} \mathbf{X}^H = \mathbf{I}$ , the channel estimate (6) takes the form  $\sqrt{\alpha} \hat{\mathbf{H}} = \frac{1}{2T} \mathbf{Y} \mathbf{X}^H = \sqrt{\alpha} \mathbf{H} + \frac{1}{2T} \mathbf{W} \mathbf{X}^H$ , where  $\frac{1}{2T} \mathbf{W} \mathbf{X}^H$  is Gaussian channel estimation error. We now analyze the  $\mathbf{H}$ -conditional correlations among the elements of the channel estimation error matrix. We begin by noticing

$$\begin{aligned} \mathbb{E} \left\{ [\frac{1}{2T} \mathbf{W} \mathbf{X}^H]_{m,p} [\frac{1}{2T} \mathbf{W} \mathbf{X}^H]_{n,q}^* \mid \mathbf{H} \right\} &= (\frac{1}{2T})^2 \mathbb{E} \left\{ \sum_k [\mathbf{W}]_{m,k} [\mathbf{X}]_{p,k}^* \sum_l [\mathbf{X}]_{q,l} [\mathbf{W}]_{n,l}^* \mid \mathbf{H} \right\} \\ &= (\frac{1}{2T})^2 \sum_{k,l} [\mathbf{X}]_{p,k}^* [\mathbf{X}]_{q,l} \mathbb{E} \{ [\mathbf{W}]_{m,k} [\mathbf{W}]_{n,l}^* \mid \mathbf{H} \}. \end{aligned} \quad (42)$$

To find  $\mathbb{E} \{ [\mathbf{W}]_{m,k} [\mathbf{W}]_{n,l}^* \mid \mathbf{H} \}$ , we recall that  $\mathbb{E} \{ [\mathbf{N}]_{m,k} [\mathbf{N}]_{n,l}^* \mid \mathbf{H} \} = \delta_{m-n} \delta_{k-l}$  and  $\mathbb{E} \{ [\mathbf{C}]_{q,k} [\mathbf{C}]_{p,l}^* \mid \mathbf{H} \} = \frac{2\kappa}{N} \delta_{q-p} \delta_{k-l}$  and  $\mathbb{E} \{ [\mathbf{E}]_{m,k} [\mathbf{E}]_{n,l}^* \mid \mathbf{H} \} = \beta [\Phi]_{m,m} \delta_{m-n} \delta_{k-l}$ , implying that

$$\begin{aligned} \mathbb{E} \{ [\mathbf{W}]_{m,k} [\mathbf{W}]_{n,l}^* \mid \mathbf{H} \} &= \alpha \sum_{q,p} [\mathbf{H}]_{m,q} [\mathbf{H}]_{n,p}^* \mathbb{E} \{ [\mathbf{C}]_{q,k} [\mathbf{C}]_{p,l}^* \mid \mathbf{H} \} + \mathbb{E} \{ [\mathbf{N}]_{m,k} [\mathbf{N}]_{n,l}^* \mid \mathbf{H} \} + \mathbb{E} \{ [\mathbf{E}]_{m,k} [\mathbf{E}]_{n,l}^* \mid \mathbf{H} \} \end{aligned} \quad (43)$$

$$= \delta_{k-l} \left( \alpha \frac{2\kappa}{N} \sum_p [\mathbf{H}]_{m,p} [\mathbf{H}]_{n,p}^* + \delta_{m-n} + \beta [\Phi]_{m,m} \delta_{m-n} \right), \quad (44)$$

which implies that

$$\begin{aligned} \mathbb{E} \left\{ [\frac{1}{2T} \mathbf{W} \mathbf{X}^H]_{m,p} [\frac{1}{2T} \mathbf{W} \mathbf{X}^H]_{n,q}^* \mid \mathbf{H} \right\} &= (\frac{1}{2T})^2 \sum_k [\mathbf{X}]_{p,k}^* [\mathbf{X}]_{q,k} \left( \alpha \frac{2\kappa}{N} \sum_p [\mathbf{H}]_{m,p} [\mathbf{H}]_{n,p}^* + \delta_{m-n} + \beta [\Phi]_{m,m} \delta_{m-n} \right) \end{aligned} \quad (45)$$

$$= \frac{1}{2T} \delta_{p-q} \left( \alpha \frac{2\kappa}{N} \sum_p [\mathbf{H}]_{m,p} [\mathbf{H}]_{n,p}^* + \delta_{m-n} + \beta [\Phi]_{m,m} \delta_{m-n} \right), \quad (46)$$

<sup>5</sup> The spatial correlation of  $\mathbf{X} = [\mathbf{x}(1), \dots, \mathbf{x}(TN)]$  is  $\mathbb{E} \{ \mathbf{x}(t) \mathbf{x}(t)^H \} = \mathbb{E} \{ \frac{1}{TN} \sum_{t=1}^{TN} \mathbf{x}(t) \mathbf{x}(t)^H \} = \mathbb{E} \{ \frac{1}{TN} \mathbf{X} \mathbf{X}^H \}$ .

where the latter expression follows from the fact that  $\sum_k [\mathbf{X}]_{p,k}^* [\mathbf{X}]_{q,k} = 2T\delta_{p-q}$ , as implied by  $\frac{1}{2T} \mathbf{X} \mathbf{X}^\mathsf{H} = \mathbf{I}$ . Equation (46) implies the estimation error is temporally white with  $\mathbf{H}$ -conditional spatial correlation

$$\mathbf{D} \triangleq \frac{1}{2T} \left( \alpha \frac{2\kappa}{N} \mathbf{H} \mathbf{H}^\mathsf{H} + \mathbf{I} + \beta \text{diag}(\Phi) \right) = \frac{1}{2T} \left( \alpha \frac{2\kappa}{N} \mathbf{H} \mathbf{H}^\mathsf{H} + \mathbf{I} + \beta \left( \alpha \frac{2(1+\kappa)}{N} \text{diag}(\mathbf{H} \mathbf{H}^\mathsf{H}) + \mathbf{I} \right) \right). \quad (47)$$

Our final claim is that the channel estimation error  $\frac{1}{2T} \mathbf{W} \mathbf{X}^\mathsf{H}$  is statistically equivalent to  $\mathbf{D}^{\frac{1}{2}} \tilde{\mathbf{H}}$ , with  $\tilde{\mathbf{H}} \in \mathbb{C}^{M \times N}$  constructed from i.i.d  $\mathcal{CN}(0, 1)$  entries. This can be seen from the following:

$$\mathbb{E} \left\{ [\mathbf{D}^{\frac{1}{2}} \tilde{\mathbf{H}}]_{m,p} [\mathbf{D}^{\frac{1}{2}} \tilde{\mathbf{H}}]_{n,q}^* \right\} = \mathbb{E} \left\{ \sum_k [\mathbf{D}^{\frac{1}{2}}]_{m,k} [\tilde{\mathbf{H}}]_{k,p} \sum_l [\mathbf{D}^{\frac{1}{2}}]_{n,l}^* [\tilde{\mathbf{H}}]_{l,q}^* \right\} \quad (48)$$

$$= \sum_{k,l} [\mathbf{D}^{\frac{1}{2}}]_{m,k} [\mathbf{D}^{\frac{1}{2}}]_{n,l}^* \mathbb{E} \left\{ [\tilde{\mathbf{H}}]_{k,p} [\tilde{\mathbf{H}}]_{l,q}^* \right\} \quad (49)$$

$$= \delta_{p-q} \sum_k [\mathbf{D}^{\frac{1}{2}}]_{m,k} [\mathbf{D}^{\frac{1}{2}}]_{n,k}^* = \delta_{p-q} [\mathbf{D}]_{m,n}, \quad (50)$$

where we used the fact that  $\mathbb{E} \left\{ [\tilde{\mathbf{H}}]_{k,p} [\tilde{\mathbf{H}}]_{l,q}^* \right\} = \delta_{k-l} \delta_{p-q}$ .

## APPENDIX B

### INTERFERENCE CANCELLATION DETAILS

In this appendix, we characterize the channel-estimate-conditioned covariance of the aggregate interference  $\mathbf{v}_r$ , whose expression was given in (11).

Recalling that  $\hat{\mathbf{D}} \triangleq \mathbb{E}\{\mathbf{D} \mid \hat{\mathbf{H}}\}$ , we first establish that  $\text{Cov}\{\mathbf{D}^{\frac{1}{2}} \tilde{\mathbf{H}} \mathbf{x} \mid \hat{\mathbf{H}}\} = \hat{\mathbf{D}} \text{tr}(\text{Cov}(\mathbf{x}))$ , which will be useful in the sequel. To show this, we examine the  $(m, n)^{th}$  element of the covariance matrix:

$$[\text{Cov}\{\mathbf{D}^{\frac{1}{2}} \tilde{\mathbf{H}} \mathbf{x} \mid \hat{\mathbf{H}}\}]_{m,n} = \mathbb{E} \left\{ [\mathbf{D}^{\frac{1}{2}} \tilde{\mathbf{H}} \mathbf{x}]_m [\mathbf{D}^{\frac{1}{2}} \tilde{\mathbf{H}} \mathbf{x}]_n^* \mid \hat{\mathbf{H}} \right\} \quad (51)$$

$$= \mathbb{E} \left\{ \sum_{p,r} [\mathbf{D}^{\frac{1}{2}}]_{m,p} [\tilde{\mathbf{H}}]_{p,r} [\mathbf{x}]_r \sum_{q,t} [\mathbf{D}^{\frac{1}{2}}]_{n,q}^* [\tilde{\mathbf{H}}]_{q,t}^* [\mathbf{x}]_t^* \mid \hat{\mathbf{H}} \right\} \quad (52)$$

$$= \sum_{p,r,q,t} \left\{ \mathbb{E} \left\{ [\mathbf{D}^{\frac{1}{2}}]_{m,p} [\mathbf{D}^{\frac{1}{2}}]_{n,q}^* \mid \hat{\mathbf{H}} \right\} \underbrace{\mathbb{E} \left\{ [\tilde{\mathbf{H}}]_{p,r} [\tilde{\mathbf{H}}]_{q,t}^* \right\}}_{\delta_{p-q} \delta_{r-t}} \mathbb{E} \left\{ [\mathbf{x}]_r [\mathbf{x}]_t^* \right\} \right\} \quad (53)$$

$$= \mathbb{E} \left\{ \sum_p [\mathbf{D}^{\frac{1}{2}}]_{m,p} [\mathbf{D}^{\frac{1}{2}}]_{n,p}^* \mid \hat{\mathbf{H}} \right\} \mathbb{E} \left\{ \sum_r [\mathbf{x}]_r [\mathbf{x}]_r^* \right\} = [\hat{\mathbf{D}}]_{m,n} \text{tr}(\text{Cov}(\mathbf{x})). \quad (54)$$

Rewriting the previous equality in matrix form, we get the desired result. As a corollary, we note that  $\mathbb{E}\{(\mathbf{D}^{\frac{1}{2}} \tilde{\mathbf{H}}) \text{Cov}\{\mathbf{x}\} (\mathbf{D}^{\frac{1}{2}} \tilde{\mathbf{H}})^\mathsf{H} \mid \hat{\mathbf{H}}\} = \hat{\mathbf{D}} \text{tr}(\text{Cov}(\mathbf{x}))$ , which will also be useful in the sequel.

Next we characterize the  $(\hat{\mathbf{H}}_{\text{sr}}, \hat{\mathbf{H}}_{\text{rr}})$ -conditional covariance of the receiver distortion  $\mathbf{e}_r$ . Recalling that  $\text{Cov}\{\mathbf{e}_r\} = \beta \text{diag}(\Phi_r)$  where  $\Phi_r = \text{Cov}\{\mathbf{u}_r\}$ , we have  $\text{Cov}\{\mathbf{e}_r \mid \hat{\mathbf{H}}_{\text{sr}}, \hat{\mathbf{H}}_{\text{rr}}\} = \beta \text{diag}(\hat{\Phi}_r)$  where  $\hat{\Phi}_r \triangleq \text{Cov}\{\mathbf{u}_r \mid \hat{\mathbf{H}}_{\text{sr}}, \hat{\mathbf{H}}_{\text{rr}}\}$ . Then, given that  $\mathbf{u}_r = \mathbf{y}_r - \mathbf{e}_r$  with  $\mathbf{y}_r$  from (10), and using the facts that

$\text{Cov}(\mathbf{x}_s + \mathbf{c}_s) = \mathbf{Q}_s + \kappa \text{diag}(\mathbf{Q}_s)$  and  $\text{Cov}(\mathbf{x}_r + \mathbf{c}_r) = \mathbf{Q}_r + \kappa \text{diag}(\mathbf{Q}_r)$ , we get

$$\begin{aligned}\hat{\Phi}_r &= \rho_r \hat{\mathbf{H}}_{sr} (\mathbf{Q}_s + \kappa \text{diag}(\mathbf{Q}_s)) \hat{\mathbf{H}}_{sr}^H + \mathbb{E} \left\{ (\mathbf{D}_{sr}^{\frac{1}{2}} \tilde{\mathbf{H}}_{sr}) (\mathbf{Q}_s + \kappa \text{diag}(\mathbf{Q}_s)) (\mathbf{D}_{sr}^{\frac{1}{2}} \tilde{\mathbf{H}}_{sr})^H \mid \hat{\mathbf{H}}_{sr} \right\} \\ &\quad + \eta_r \hat{\mathbf{H}}_{rr} (\mathbf{Q}_r + \kappa \text{diag}(\mathbf{Q}_r)) \hat{\mathbf{H}}_{rr}^H + \mathbb{E} \left\{ (\mathbf{D}_{rr}^{\frac{1}{2}} \tilde{\mathbf{H}}_{rr}) (\mathbf{Q}_r + \kappa \text{diag}(\mathbf{Q}_r)) \times (\mathbf{D}_{rr}^{\frac{1}{2}} \tilde{\mathbf{H}}_{rr})^H \mid \hat{\mathbf{H}}_{rr} \right\} + \mathbf{I} \\ &= \rho_r \hat{\mathbf{H}}_{sr} (\mathbf{Q}_s + \kappa \text{diag}(\mathbf{Q}_s)) \hat{\mathbf{H}}_{sr}^H + \hat{\mathbf{D}}_{sr} \text{tr}(\mathbf{Q}_s + \kappa \text{diag}(\mathbf{Q}_s)) + \eta_r \hat{\mathbf{H}}_{rr} (\mathbf{Q}_r + \kappa \text{diag}(\mathbf{Q}_r)) \hat{\mathbf{H}}_{rr}^H \\ &\quad + \hat{\mathbf{D}}_{rr} \text{tr}(\mathbf{Q}_r + \kappa \text{diag}(\mathbf{Q}_r)) + \mathbf{I}.\end{aligned}\quad (56)$$

$$\begin{aligned}\text{Then } \hat{\Phi}_r &= \rho_r \hat{\mathbf{H}}_{sr} (\mathbf{Q}_s + \kappa \text{diag}(\mathbf{Q}_s)) \hat{\mathbf{H}}_{sr}^H + (1 + \kappa) \hat{\mathbf{D}}_{sr} \text{tr}(\mathbf{Q}_s) + \eta_r \hat{\mathbf{H}}_{rr} (\mathbf{Q}_r + \kappa \text{diag}(\mathbf{Q}_r)) \hat{\mathbf{H}}_{rr}^H \\ &\quad + (1 + \kappa) \hat{\mathbf{D}}_{rr} \text{tr}(\mathbf{Q}_r) + \mathbf{I}\end{aligned}\quad (57)$$

$$\approx \rho_r \hat{\mathbf{H}}_{sr} \mathbf{Q}_s \hat{\mathbf{H}}_{sr}^H + \hat{\mathbf{D}}_{sr} \text{tr}(\mathbf{Q}_s) + \eta_r \hat{\mathbf{H}}_{rr} \mathbf{Q}_r \hat{\mathbf{H}}_{rr}^H + \hat{\mathbf{D}}_{rr} \text{tr}(\mathbf{Q}_r) + \mathbf{I},\quad (58)$$

where, for the approximation, we assumed  $\kappa \ll 1$ . Thus,

$$\text{Cov}\{e_r \mid \hat{\mathbf{H}}_{sr}, \hat{\mathbf{H}}_{rr}\} \approx \beta (\rho_r \text{diag}(\hat{\mathbf{H}}_{sr} \mathbf{Q}_s \hat{\mathbf{H}}_{sr}^H) + \hat{\mathbf{D}}_{sr} \text{tr}(\mathbf{Q}_s) + \eta_r \text{diag}(\hat{\mathbf{H}}_{rr} \mathbf{Q}_r \hat{\mathbf{H}}_{rr}^H) + \hat{\mathbf{D}}_{rr} \text{tr}(\mathbf{Q}_r) + \mathbf{I})\quad (59)$$

Finally we are ready to characterize  $\hat{\Sigma}_r$ , the  $(\hat{\mathbf{H}}_{sr}, \hat{\mathbf{H}}_{rr})$ -conditional covariance of  $\mathbf{v}_r$ . From (11),

$$\begin{aligned}\hat{\Sigma}_r &= \kappa \rho_r \mathbb{E} \left\{ \mathbf{H}_{sr} \text{diag}(\mathbf{Q}_s) \mathbf{H}_{sr}^H \mid \hat{\mathbf{H}}_{sr} \right\} + \hat{\mathbf{D}}_{sr} \text{tr}(\mathbf{Q}_s) + \kappa \eta_r \mathbb{E} \left\{ \mathbf{H}_{rr} \text{diag}(\mathbf{Q}_r) \mathbf{H}_{rr}^H \mid \hat{\mathbf{H}}_{rr} \right\} + \hat{\mathbf{D}}_{rr} \text{tr}(\mathbf{Q}_r) \\ &\quad + \mathbf{I} + \text{Cov}\{e_r \mid \hat{\mathbf{H}}_{sr}, \hat{\mathbf{H}}_{rr}\}\end{aligned}\quad (60)$$

$$\begin{aligned}&= \kappa \rho_r \hat{\mathbf{H}}_{sr} \text{diag}(\mathbf{Q}_s) \hat{\mathbf{H}}_{sr}^H + \mathbf{I} + \text{Cov}\{e_s \mid \hat{\mathbf{H}}_{sr}, \hat{\mathbf{H}}_{rr}\} + \kappa \mathbb{E} \left\{ (\mathbf{D}_{sr}^{\frac{1}{2}} \tilde{\mathbf{H}}_{sr}) \text{diag}(\mathbf{Q}_s) (\mathbf{D}_{sr}^{\frac{1}{2}} \tilde{\mathbf{H}}_{sr})^H \mid \hat{\mathbf{H}}_{sr} \right\} \\ &\quad + \hat{\mathbf{D}}_{sr} \text{tr}(\mathbf{Q}_s) + \hat{\mathbf{D}}_{rr} \text{tr}(\mathbf{Q}_r) + \kappa \eta_r \hat{\mathbf{H}}_{rr} \text{diag}(\mathbf{Q}_r) \hat{\mathbf{H}}_{rr}^H + \kappa \mathbb{E} \left\{ (\mathbf{D}_{rr}^{\frac{1}{2}} \tilde{\mathbf{H}}_{rr}) \text{diag}(\mathbf{Q}_r) (\mathbf{D}_{rr}^{\frac{1}{2}} \tilde{\mathbf{H}}_{rr})^H \mid \hat{\mathbf{H}}_{rr} \right\} \\ &= \kappa \rho_r \hat{\mathbf{H}}_{sr} \text{diag}(\mathbf{Q}_s) \hat{\mathbf{H}}_{sr}^H + (1 + \kappa) \hat{\mathbf{D}}_{sr} \text{tr}(\mathbf{Q}_s) + \kappa \eta_r \hat{\mathbf{H}}_{rr} \text{diag}(\mathbf{Q}_r) \hat{\mathbf{H}}_{rr}^H + (1 + \kappa) \hat{\mathbf{D}}_{rr} \text{tr}(\mathbf{Q}_r) \\ &\quad + \mathbf{I} + \text{Cov}\{e_s \mid \hat{\mathbf{H}}_{sr}, \hat{\mathbf{H}}_{rr}\}\end{aligned}\quad (61)$$

$$\begin{aligned}&\approx \mathbf{I} + \kappa \rho_r \hat{\mathbf{H}}_{sr} \text{diag}(\mathbf{Q}_s) \hat{\mathbf{H}}_{sr}^H + \hat{\mathbf{D}}_{sr} \text{tr}(\mathbf{Q}_s) + \kappa \eta_r \hat{\mathbf{H}}_{rr} \text{diag}(\mathbf{Q}_r) \hat{\mathbf{H}}_{rr}^H + \hat{\mathbf{D}}_{rr} \text{tr}(\mathbf{Q}_r) \\ &\quad + \beta \rho_r \text{diag}(\hat{\mathbf{H}}_{sr} \mathbf{Q}_s \hat{\mathbf{H}}_{sr}^H) + \beta \eta_r \text{diag}(\hat{\mathbf{H}}_{rr} \mathbf{Q}_r \hat{\mathbf{H}}_{rr}^H),\end{aligned}\quad (62)$$

where, for the approximation, we assumed  $\kappa \ll 1$  and  $\beta \ll 1$ , and we leveraged (59).

## APPENDIX C

### GRADIENT DETAILS

In this appendix, we derive an expression for the gradient  $\nabla_{\mathbf{Q}_r[l]} \underline{I}(\mathbf{Q}, \zeta)$  by first deriving an expression for the derivative  $\partial \underline{I} / \partial \mathbf{Q}_r[l]$  and then using the fact that  $\nabla_{\mathbf{Q}_r[l]} \underline{I} = 2(\partial \underline{I} / \partial \mathbf{Q}_r[l])^*$ .

To do this, we first consider the related problem of computing the derivative  $\partial \det(\mathbf{Y})/\partial \mathbf{X}$ , where

$$\mathbf{Y} \triangleq \mathbf{C} \operatorname{diag}(\mathbf{X}) \mathbf{D} + \operatorname{diag}(\mathbf{E} \mathbf{X} \mathbf{F}) + \mathbf{G} \operatorname{tr}(\mathbf{X}) + \mathbf{Z}, \quad (63)$$

and where (63) can be written elementwise as

$$[\mathbf{Y}]_{i,j} = \sum_{m,n} [\mathbf{C}]_{i,m} [\mathbf{X}]_{m,n} [\mathbf{D}]_{n,j} \delta_{m-n} + [\mathbf{Z}]_{i,j} + \sum_{p,q} [\mathbf{E}]_{i,p} [\mathbf{X}]_{p,q} [\mathbf{F}]_{q,j} \delta_{i-j} + [\mathbf{G}]_{i,j} \sum_t [\mathbf{X}]_{t,t}. \quad (64)$$

Notice that, for  $\mathbf{V}_{r,s}$  defined as a zero-valued matrix except for a unity element at row  $r$  and column  $s$ , we have  $\frac{\partial \det(\mathbf{Y})}{\partial \mathbf{X}} = \sum_{r,s} \mathbf{V}_{r,s} \frac{\partial \det(\mathbf{Y})}{\partial [\mathbf{X}]_{r,s}} = \sum_{r,s} \mathbf{V}_{r,s} \sum_{i,j} \frac{\partial \det(\mathbf{Y})}{\partial [\mathbf{Y}]_{i,j}} \frac{\partial [\mathbf{Y}]_{i,j}}{\partial [\mathbf{X}]_{r,s}}$ . Then, using (64), we get

$$\frac{\partial \det(\mathbf{Y})}{\partial \mathbf{X}} = \sum_{r,s} \mathbf{V}_{r,s} \sum_{i,j} \frac{\partial \det(\mathbf{Y})}{\partial [\mathbf{Y}]_{i,j}} [[\mathbf{C}]_{i,r} [\mathbf{D}]_{s,j} \delta_{r-s} + [\mathbf{E}]_{i,r} [\mathbf{F}]_{s,j} \delta_{i-j} + [\mathbf{G}]_{i,j} \delta_{r-s}]] \quad (65)$$

$$= \operatorname{diag}(\mathbf{D} [\frac{\partial \det \mathbf{Y}}{\partial \mathbf{Y}}]^\top \mathbf{C}) + [\mathbf{F} \operatorname{diag}(\frac{\partial \det \mathbf{Y}}{\partial \mathbf{Y}})^\top \mathbf{E}]^\top + \operatorname{sum}[\mathbf{G} \odot [\frac{\partial \det \mathbf{Y}}{\partial \mathbf{Y}}]] \mathbf{I} \quad (66)$$

$$= \det(\mathbf{Y}) \{ \operatorname{diag}(\mathbf{D} \mathbf{Y}^{-1} \mathbf{C}) + [\mathbf{F} \operatorname{diag}(\mathbf{Y}^{-1}) \mathbf{E}]^\top + \operatorname{sum}(\mathbf{G} \odot (\mathbf{Y}^{-1})^\top) \mathbf{I} \}, \quad (67)$$

where, for the last step, we used the fact that  $\partial \det(\mathbf{Y})/\partial \mathbf{Y} = \det(\mathbf{Y})(\mathbf{Y}^{-1})^\top$ .

Applying (67) to (20), we can obtain an expression for  $\partial \underline{I}/\partial \mathbf{Q}_r[l]$ . To do so, we think of  $\mathbf{Z}$  in (63) as representing the terms in  $\underline{I}$  that have zero derivative with respect to  $\mathbf{Q}_r[l]$ . Using  $\mathbf{S}_d[l]$  and  $\mathbf{S}_r[l]$  defined in (35)-(36), and recalling the expression for  $\hat{\Sigma}_d[l]$  in (13), the result is

$$\begin{aligned} & \frac{\partial}{\partial \mathbf{Q}_r[l]} \underline{I}(\mathbf{Q}_s[1], \mathbf{Q}_s[2], \mathbf{Q}_r[1], \mathbf{Q}_r[2], \zeta) \\ &= \frac{\partial}{\partial \mathbf{Q}_r[l]} \left\{ \frac{1-\zeta}{2} (\log \det(\mathbf{S}_d[l]) - \log \det(\hat{\Sigma}_d[l])) + \frac{\zeta}{2} (\log \det(\mathbf{S}_r[l]) - \log \det(\hat{\Sigma}_r[l])) \right\} \quad (68) \\ &= \frac{\partial}{\partial \mathbf{Q}_r[l]} \frac{1}{2} \left\{ (1-\zeta) \log \det \left( \rho_d \hat{\mathbf{H}}_{rd} \mathbf{Q}_r[l] \hat{\mathbf{H}}_{rd}^\top + \kappa \rho_d \hat{\mathbf{H}}_{rd} \operatorname{diag}(\mathbf{Q}_r[l]) \hat{\mathbf{H}}_{rd}^\top \right. \right. \\ & \quad \left. \left. + \beta \rho_d \operatorname{diag}(\hat{\mathbf{H}}_{rd} \mathbf{Q}_r[l] \hat{\mathbf{H}}_{rd}^\top) + \hat{\mathbf{D}}_{rd} \operatorname{tr} \mathbf{Q}_r[l] + \mathbf{Z}_1[l] \right) \right. \\ & \quad \left. - (1-\zeta) \log \det \left( \kappa \rho_d \hat{\mathbf{H}}_{rd} \operatorname{diag}(\mathbf{Q}_r[l]) \hat{\mathbf{H}}_{rd}^\top + \beta \rho_d \operatorname{diag}(\hat{\mathbf{H}}_{rd} \mathbf{Q}_r[l] \hat{\mathbf{H}}_{rd}^\top) + \hat{\mathbf{D}}_{rd} \operatorname{tr} \mathbf{Q}_r[l] + \mathbf{Z}_2[l] \right) \right. \\ & \quad \left. + \zeta \log \det \left( \beta \eta_r \operatorname{diag}(\hat{\mathbf{H}}_{rd} \mathbf{Q}_r[l] \hat{\mathbf{H}}_{rd}^\top) + \kappa \eta_r \hat{\mathbf{H}}_{rr} \operatorname{diag}(\mathbf{Q}_r[l]) \hat{\mathbf{H}}_{rr}^\top + \hat{\mathbf{D}}_{rr} \operatorname{tr} \mathbf{Q}_r[l] + \mathbf{Z}_3[l] \right) \right. \\ & \quad \left. - \zeta \log \det \left( \beta \eta_r \operatorname{diag}(\hat{\mathbf{H}}_{rd} \mathbf{Q}_r[l] \hat{\mathbf{H}}_{rd}^\top) + \kappa \eta_r \hat{\mathbf{H}}_{rr} \operatorname{diag}(\mathbf{Q}_r[l]) \hat{\mathbf{H}}_{rr}^\top + \hat{\mathbf{D}}_{rr} \operatorname{tr} \mathbf{Q}_r[l] + \mathbf{Z}_4[l] \right) \right\} \\ &= \frac{(1-\zeta)\rho_d}{\ln 2} \left\{ (\hat{\mathbf{H}}_{rd}^\top [\mathbf{S}_d^{-1}[l] + \beta \operatorname{diag}(\mathbf{S}_d^{-1}[l] - \hat{\Sigma}_d^{-1}[l])] \hat{\mathbf{H}}_{rd})^\top + \kappa \operatorname{diag}(\hat{\mathbf{H}}_{rd}^\top (\mathbf{S}_d^{-1}[l] - \hat{\Sigma}_d^{-1}[l]) \hat{\mathbf{H}}_{rd}) \right\} \\ & \quad + \frac{1-\zeta}{\ln 2} \operatorname{sum}(\hat{\mathbf{D}}_{rd} \odot (\mathbf{S}_d^{-1}[l] - \hat{\Sigma}_d^{-1}[l])^\top) \mathbf{I} + \frac{\zeta \eta_r}{\ln 2} \left\{ \kappa \operatorname{diag}(\hat{\mathbf{H}}_{rr}^\top (\mathbf{S}_r^{-1}[l] - \hat{\Sigma}_r^{-1}[l]) \hat{\mathbf{H}}_{rr}) \right. \\ & \quad \left. + \beta (\hat{\mathbf{H}}_{rd}^\top \operatorname{diag}(\mathbf{S}_r^{-1}[l] - \hat{\Sigma}_r^{-1}[l]) \hat{\mathbf{H}}_{rd})^\top \right\} + \frac{\zeta}{\ln 2} \operatorname{sum}(\hat{\mathbf{D}}_{rr} \odot (\mathbf{S}_r^{-1}[l] - \hat{\Sigma}_r^{-1}[l])^\top) \mathbf{I}. \quad (69) \end{aligned}$$

Finally, using  $\mathbf{G}_r[l] = 2(\partial \underline{I}/\partial \mathbf{Q}_r[l])^*$ , and leveraging the fact that  $\mathbf{S}_d[l]$ ,  $\mathbf{S}_r[l]$ ,  $\hat{\Sigma}_d[l]$ , and  $\hat{\Sigma}_r[l]$  are Hermitian matrices, we get the expression for  $\mathbf{G}_r[l]$  in (34). A similar expression results for  $\mathbf{G}_s[l]$ .

## REFERENCES

- [1] Y. Hua, "An overview of beamforming and power allocation for MIMO relays," in *Proc. IEEE Military Commun. Conf.*, (San Jose, CA), pp. 375–380, Nov. 2010.
- [2] B. Wang, J. Zhang, and A. Høst-Madsen, "On the capacity of MIMO relay channels," *IEEE Trans. Inform. Theory*, vol. 51, pp. 29–43, Jan. 2005.
- [3] S. Simoens, O. Muñoz-Medina, J. Vidal, and A. del Coso, "On the Gaussian MIMO relay channel with full channel state information," *IEEE Trans. Signal Process.*, vol. 57, pp. 3588–3599, Sep. 2009.
- [4] D. W. Bliss, P. A. Parker, and A. R. Margetts, "Simultaneous transmission and reception for improved wireless network performance," in *Proc. IEEE Workshop Statist. Signal Process.*, (Madison, WI), pp. 478–482, Aug. 2007.
- [5] P. Larsson and M. Prytz, "MIMO on-frequency repeater with self-interference cancellation and mitigation," in *Proc. IEEE Veh. Tech. Conf.*, (Barcelona, Spain), Apr. 2009.
- [6] T. Riihonen, S. Werner, and R. Wichman, "Spatial loop interference suppression in full-duplex MIMO relays," in *Proc. Asilomar Conf. Signals Syst. Comput.*, (Pacific Grove, CA), Nov. 2009.
- [7] T. Riihonen, S. Werner, and R. Wichman, "Residual self-interference in full-duplex MIMO relays after null-space projection and cancellation," in *Proc. Asilomar Conf. Signals Syst. Comput.*, (Pacific Grove, CA), Nov. 2010.
- [8] T. Riihonen, A. Balakrishnan, K. Haneda, S. Wyne, S. Werner, and R. Wichman, "Optimal eigenbeamforming for suppressing self-interference in full-duplex MIMO relays," in *Proc. Conf. Inform. Science & Syst.*, (Baltimore, MD), Mar. 2011.
- [9] S. Sohaib and Daniel K.C. So, "Asynchronous polarized cooperative MIMO communication," in *Proc. IEEE Veh. Tech. Conf.*, (Barcelona, Spain), Apr. 2009.
- [10] J. Sangiamwong, T. Asai, J. Hagiwara, Y. Okumura, and T. Ohya, "Joint multi-filter design for full-duplex MU-MIMO relaying," in *Proc. IEEE Veh. Tech. Conf.*, (Barcelona, Spain), Apr. 2009.
- [11] B. Chun, E.-R. Jeong, J. Joung, Y. Oh, and Y. H. Lee, "Pre-nulling for self-interference suppression in full-duplex relays," in *Proc. APSIPA Annual Summit and Conf.*, (Sapporo, Japan), Oct. 2009.
- [12] B. Chun and Y. H. Lee, "A spatial self-interference nullification method for full duplex amplify-and-forward MIMO relays," in *Proc. IEEE Wireless Commun. & Netw. Conf.*, (Sydney, Australia), Apr. 2010.
- [13] P. Lioliou, M. Viberg, M. Coldrey, and F. Athley, "Self-interference suppression in full-duplex MIMO relays," in *Proc. Asilomar Conf. Signals Syst. Comput.*, (Pacific Grove, CA), Oct. 2010.
- [14] H. Suzuki, T. V. A. Tran, I. B. Collings, G. Daniels, and M. Hedley, "Transmitter noise effect on the performance of a MIMO-OFDM hardware implementation achieving improved coverage," *IEEE J. Sel. Areas Commun.*, vol. 26, pp. 867–876, Aug. 2008.
- [15] W. Namgoong, "Modeling and analysis of nonlinearities and mismatches in AC-coupled direct-conversion receiver," *IEEE Trans. Wireless Commun.*, vol. 4, pp. 163–173, Jan. 2005.
- [16] B. Hassibi and B. M. Hochwald, "How much training is needed in multiple-antenna wireless links," *IEEE Trans. Inform. Theory*, vol. 49, pp. 951–963, Apr. 2003.
- [17] D. Tse and P. Viswanath, *Fundamentals of Wireless Communication*. New York: Cambridge University Press, 2005.
- [18] D. Bertsekas, *Nonlinear Programming*. Athena Scientific, 2nd ed., 1999.
- [19] Y. Rong and Y. Hua, "Optimal power schedule for distributed MIMO links," *IEEE Trans. Wireless Commun.*, vol. 7, pp. 2896–2900, Aug. 2008.

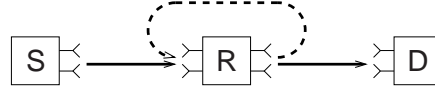


Fig. 1. Full-duplex MIMO relaying from source to destination. Solid lines denote desired propagation and dashed line denotes self-interference.

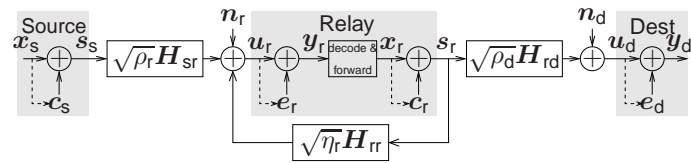


Fig. 2. Our model of full-duplex MIMO relaying under limited transmitter/receiver-DR. The dashed lines denote statistical dependence.

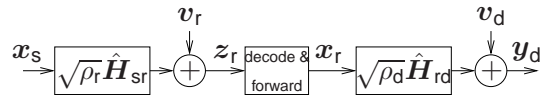


Fig. 3. Equivalent model of full-duplex MIMO relaying under limited-DR and channel estimation error.

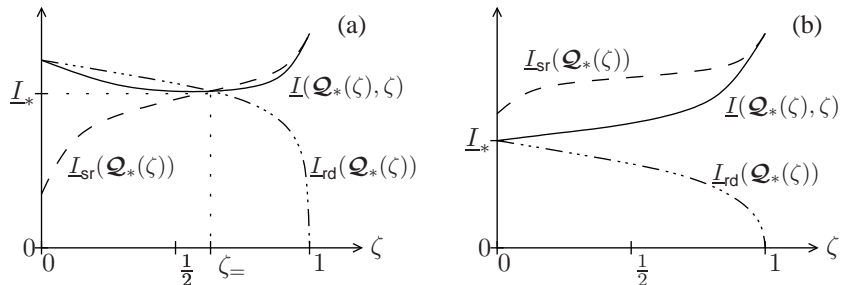


Fig. 4. Illustrative examples of  $\underline{I}$  versus  $\zeta$  in  $\zeta$ -weighted-sum-rate optimization yielding (a) a link-equalizing solution, (b) no link-equalizing solution.

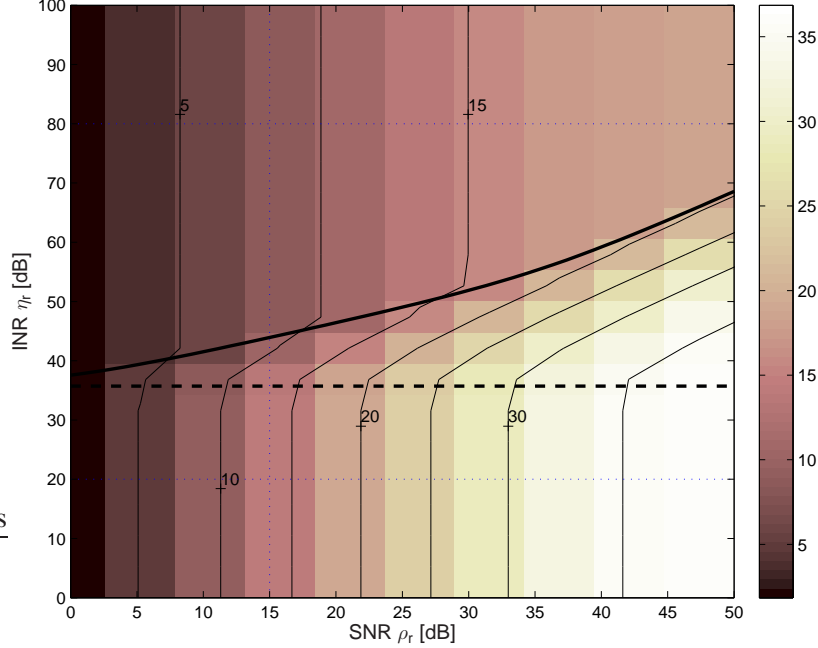


Fig. 5. Contour plot of the approximated achievable rate  $I_*$  versus relay SNR  $\rho_r$  and INR  $\eta_r$ , for  $N = 3$ ,  $M = 4$ ,  $\beta = \kappa = -40$ dB, and  $\rho_r/\rho_d = 2$ . The horizontal dashed line shows the INR  $\eta_{\text{crit}}$ , and the dark curve shows the boundary between full- and half-duplex regimes described in (41).

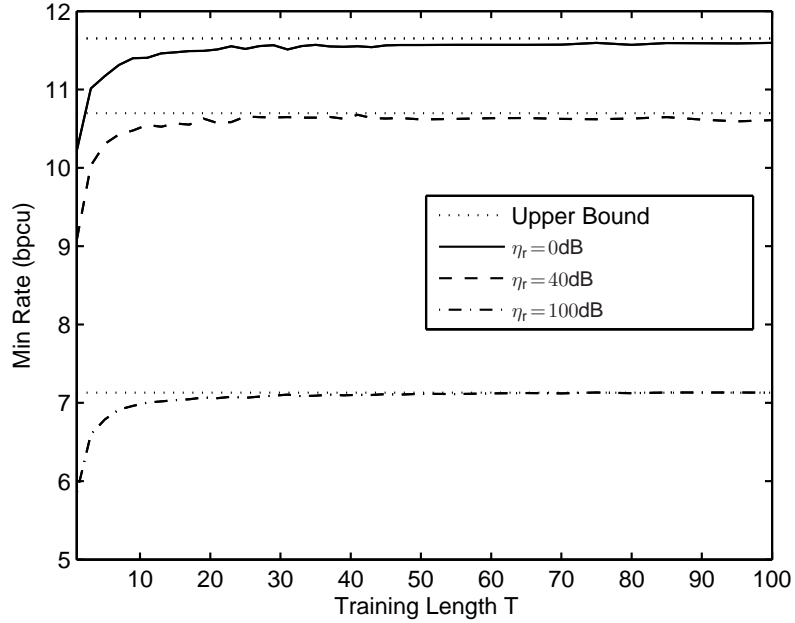


Fig. 6. Achievable-rate lower bound  $\underline{I}(\mathcal{Q})$  for TCO-2-IC versus training interval  $T$ . Here,  $N = 3$ ,  $M = 4$ ,  $\beta = \kappa = -40$ dB,  $\rho_r = 15$ dB, and  $\rho_r/\rho_d = 2$ . Also shown is the corresponding upper bound  $\bar{I}(\mathcal{Q})$  for each value of  $\eta_r$ .

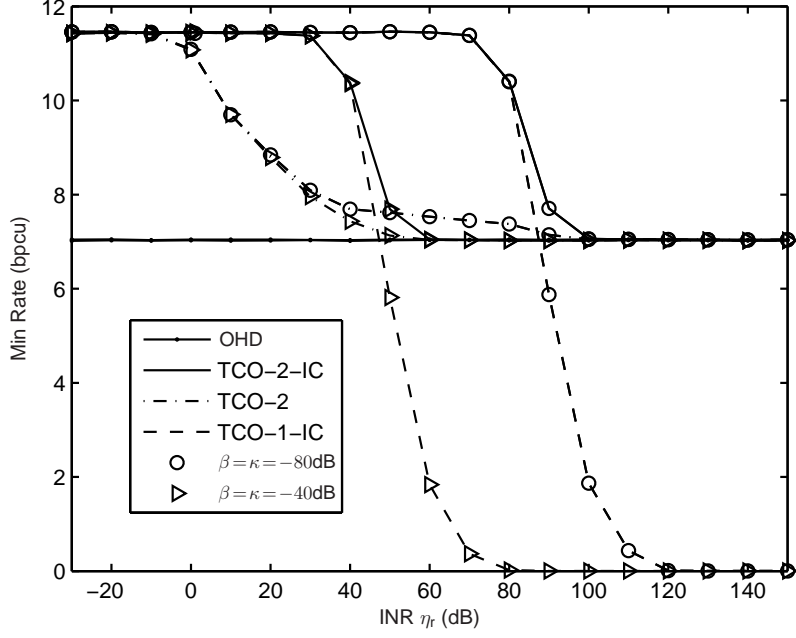


Fig. 7. Achievable-rate lower bound  $\underline{I}(\mathcal{Q})$  for TCO-2-IC, TCO-2, TCO-1-IC, and OHD versus INR  $\eta_r$ . Here,  $N = 3$ ,  $M = 4$ ,  $\rho_r = 15$ dB,  $\rho_r/\rho_d = 2$ , and  $T = 50$ . OHD is plotted for  $\beta = \kappa = -40$ dB, but was observed to give nearly identical rate for  $\beta = \kappa = -80$ dB.

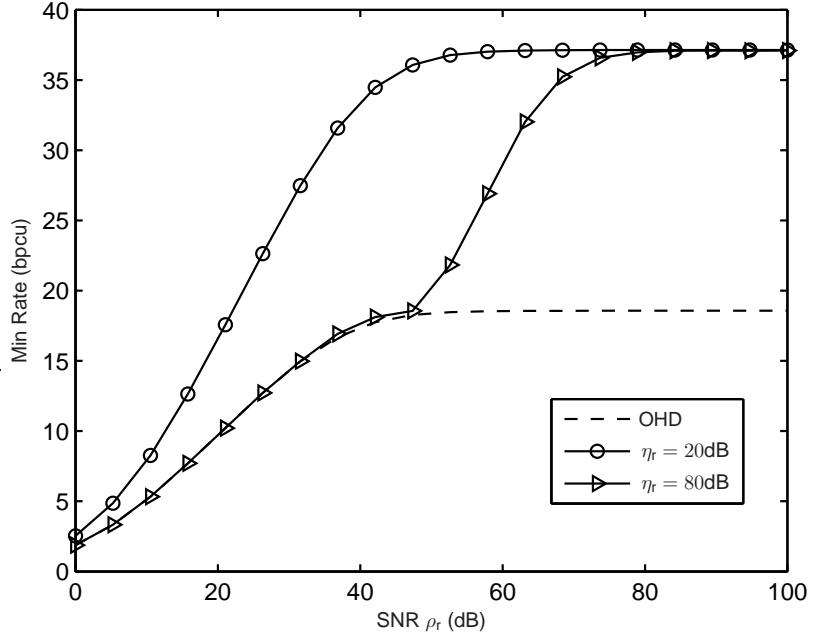


Fig. 8. Achievable-rate lower bound  $\underline{I}(\mathcal{Q})$  for TCO-2-IC and OHD versus SNR  $\rho_r$ . Here,  $\rho_r/\rho_d = 2$ ,  $N = 3$ ,  $M = 4$ ,  $\beta = \kappa = -40$ dB, and  $T = 50$ .

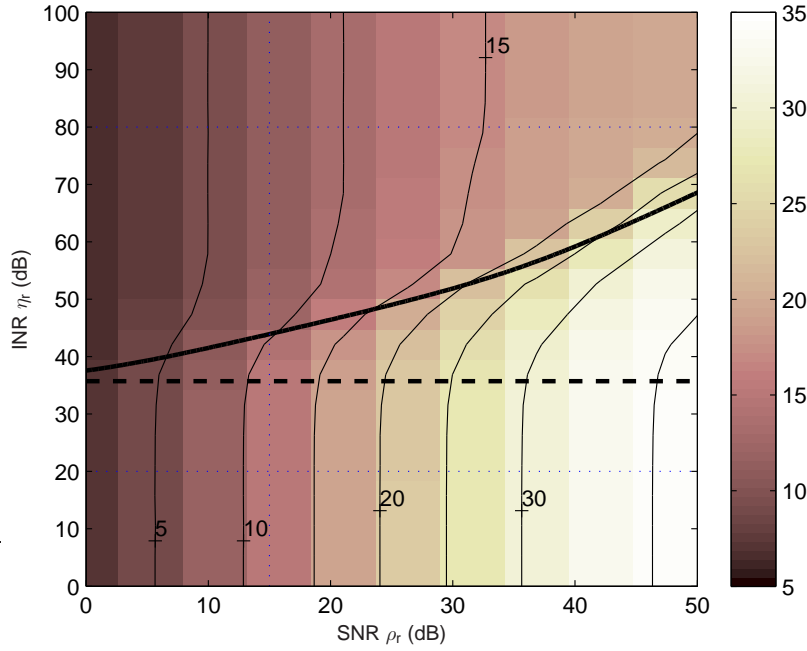


Fig. 9. Contour plot of the achievable-rate lower bound  $\underline{I}(\mathcal{Q})$  for TCO-2-IC versus INR  $\eta_r$  and SNR  $\rho_r$ , for  $\rho_d = \rho_r/2$ ,  $N = 3$ ,  $M = 4$ , and  $\beta = \kappa = -40$  dB. The dark curve (i.e., approximate full/half-duplex boundary) and dashed line (i.e., critical INR  $\eta_{\text{crit}}$ ) are the same as in Fig. 5.

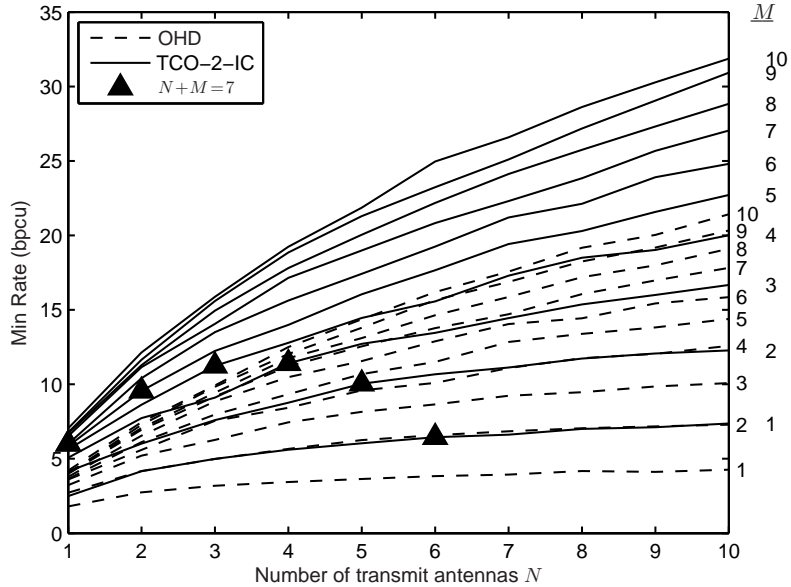


Fig. 10. Achievable-rate lower bound  $\underline{I}(\mathcal{Q})$  for TCO-2-IC and OHD versus number of transmit antennas  $N$  with various numbers of receive antennas  $M$ . Here,  $\rho_r = 15$  dB,  $\rho_r/\rho_d = 2$ ,  $\eta_r = 40$  dB,  $\beta = \kappa = -40$  dB, and  $T = 50$ .